

# Targeting TBK1 to overcome resistance to cancer immunotherapy

<https://doi.org/10.1038/s41586-023-05704-6>

Received: 16 July 2021

Accepted: 4 January 2023

Published online: 12 January 2023

 Check for updates

Yi Sun<sup>1</sup>, Or-yam Revach<sup>1</sup>, Seth Anderson<sup>2</sup>, Emily A. Kessler<sup>2</sup>, Clara H. Wolfe<sup>2</sup>, Anne Jenney<sup>3</sup>, Caitlin E. Mills<sup>3</sup>, Emily J. Robitschek<sup>2</sup>, Thomas G. R. Davis<sup>2</sup>, Sarah Kim<sup>2</sup>, Amina Fu<sup>1</sup>, Xiang Ma<sup>1</sup>, Jia Gwee<sup>1</sup>, Payal Tiwari<sup>2</sup>, Peter P. Du<sup>2</sup>, Princy Sindurakar<sup>1</sup>, Jun Tian<sup>1</sup>, Arnav Mehta<sup>1,2,4</sup>, Alexis M. Schneider<sup>2,5</sup>, Keren Yizhak<sup>6</sup>, Moshe Sade-Feldman<sup>1,2</sup>, Thomas LaSalle<sup>1</sup>, Tatyana Sharova<sup>7</sup>, Hongyan Xie<sup>1</sup>, Shuming Liu<sup>3</sup>, William A. Michaud<sup>7</sup>, Rodrigo Saad-Beretta<sup>1</sup>, Kathleen B. Yates<sup>1,2</sup>, Arvin Iracheta-Vellve<sup>2</sup>, Johan K. E. Spetz<sup>3,8,9</sup>, Xingping Qin<sup>3,8,9</sup>, Kristopher A. Sarosiek<sup>3,8,9</sup>, Gao Zhang<sup>10,11,12</sup>, Jong Wook Kim<sup>13,14,15</sup>, Mack Y. Su<sup>16</sup>, Angelina M. Cicerchia<sup>1</sup>, Martin Q. Rasmussen<sup>1</sup>, Samuel J. Klemperer<sup>1</sup>, Dejan Juric<sup>1</sup>, Sara I. Pai<sup>7,17</sup>, David M. Miller<sup>1,18</sup>, Anita Giobbie-Hurder<sup>19</sup>, Jonathan H. Chen<sup>1,2,20</sup>, Karin Pelka<sup>1,2</sup>, Dennie T. Frederick<sup>1</sup>, Susanna Stinson<sup>21</sup>, Elena Ivanova<sup>4,22</sup>, Amir R. Aref<sup>4,22,23</sup>, Cloud P. Paweletz<sup>4,22</sup>, David A. Barbie<sup>4,22</sup>, Debattama R. Sen<sup>1</sup>, David E. Fisher<sup>16</sup>, Ryan B. Corcoran<sup>1</sup>, Nir Hacohen<sup>1,2</sup>, Peter K. Sorger<sup>3</sup>, Keith T. Flaherty<sup>1</sup>, Genevieve M. Boland<sup>2,7</sup>, Robert T. Manguso<sup>1,2,24</sup> & Russell W. Jenkins<sup>1,2,3,24</sup>✉

Despite the success of PD-1 blockade in melanoma and other cancers, effective treatment strategies to overcome resistance to cancer immunotherapy are lacking<sup>1,2</sup>. Here we identify the innate immune kinase TANK-binding kinase 1 (*TBK1*)<sup>3</sup> as a candidate immune-evasion gene in a pooled genetic screen<sup>4</sup>. Using a suite of genetic and pharmacological tools across multiple experimental model systems, we confirm a role for *TBK1* as an immune-evasion gene. Targeting *TBK1* enhances responses to PD-1 blockade by decreasing the cytotoxicity threshold to effector cytokines (TNF and IFN $\gamma$ ). *TBK1* inhibition in combination with PD-1 blockade also demonstrated efficacy using patient-derived tumour models, with concordant findings in matched patient-derived organotypic tumour spheroids and matched patient-derived organoids. Tumour cells lacking *TBK1* are primed to undergo RIPK- and caspase-dependent cell death in response to TNF and IFN $\gamma$  in a JAK–STAT-dependent manner. Taken together, our results demonstrate that targeting *TBK1* is an effective strategy to overcome resistance to cancer immunotherapy.

Cancer immunotherapy with immune checkpoint blockade (ICB) has transformed the treatment of advanced melanoma and other cancers, although overcoming resistance remains a central challenge<sup>1,2</sup>. There are currently no approved therapies for patients with innate or acquired resistance to ICB. Clinical trials evaluating new immune modulatory agents in combination with anti-PD-1 and anti-PD-L1 therapies to overcome primary resistance are already underway<sup>5</sup>. Recently, the results of two phase III, placebo-controlled, randomized clinical trials comparing promising combination strategies were reported, neither showing a survival benefit compared with single-agent PD-1 blockade<sup>6,7</sup>,

prompting renewed focus on the preclinical and early-phase clinical development of combination strategies.

Approaches to unbiased target identification include loss-of-function genetic screens using CRISPR–Cas9 genome editing, which have successfully nominated targets to enhance anti-tumour immune responses<sup>4,8</sup>. Pooled in vivo and in vitro CRISPR–Cas9-based screening have nominated several tumour-intrinsic drivers of resistance to immunotherapy<sup>4,8–11</sup>, but therapeutic applications of these findings remain limited.

TANK-binding kinase 1 (*TBK1*) is a multifunctional serine/threonine kinase with an established role coordinating innate immune responses

<sup>1</sup>Massachusetts General Hospital Cancer Center, Department of Medicine, Massachusetts General Hospital, Harvard Medical School, Boston, MA, USA. <sup>2</sup>Broad Institute of MIT and Harvard, Cambridge, MA, USA. <sup>3</sup>Laboratory of Systems Pharmacology, Harvard Program in Therapeutic Sciences, Harvard Medical School, Boston, MA, USA. <sup>4</sup>Department of Medical Oncology, Dana-Farber Cancer Institute, Boston, MA, USA. <sup>5</sup>Department of Biological Engineering, Massachusetts Institute of Technology, Cambridge, MA, USA. <sup>6</sup>Department of Cell Biology and Cancer Science, Rappaport Faculty of Medicine, Institute of Technology, Technion, Haifa, Israel. <sup>7</sup>Division of Surgical Oncology, Department of Surgery, Massachusetts General Hospital Cancer Center, Harvard Medical School, Boston, MA, USA. <sup>8</sup>Molecular and Integrative Physiological Sciences Program, Harvard School of Public Health, Boston, MA, USA. <sup>9</sup>John B. Little Center for Radiation Sciences, Harvard School of Public Health, Boston, MA, USA. <sup>10</sup>Molecular and Cellular Oncogenesis Program, The Wistar Institute, Philadelphia, PA, USA. <sup>11</sup>Preston Robert Tisch Brain Tumor Center, Department of Neurosurgery, Duke University School of Medicine, Durham, NC, USA. <sup>12</sup>Preston Robert Tisch Brain Tumor Center, Department of Pathology, Duke University School of Medicine, Durham, NC, USA. <sup>13</sup>Moore's Cancer Center, UC San Diego, La Jolla, CA, USA. <sup>14</sup>Center for Novel Therapeutics, UC San Diego, La Jolla, CA, USA. <sup>15</sup>Department of Medicine, UC San Diego, La Jolla, CA, USA. <sup>16</sup>Cutaneous Biology Research Center, Department of Dermatology, Massachusetts General Hospital and Harvard Medical School, Boston, MA, USA. <sup>17</sup>Center for Systems Biology, Massachusetts General Hospital, Boston, MA, USA. <sup>18</sup>Department of Dermatology, Massachusetts General Hospital and Harvard Medical School, Boston, MA, USA. <sup>19</sup>Division of Biostatistics, Department of Data Sciences, Dana-Farber Cancer Institute, Boston, MA, USA. <sup>20</sup>Department of Pathology, Massachusetts General Hospital, Boston, MA, USA. <sup>21</sup>Gilead Sciences, Foster City, CA, USA. <sup>22</sup>Belfer Center for Applied Cancer Science, Dana-Farber Cancer Institute, Boston, MA, USA. <sup>23</sup>Xspera Biosciences, Boston, MA, USA. <sup>24</sup>These authors jointly supervised this work: Robert T. Manguso, Russell W. Jenkins. ✉e-mail: rjenkins@mgh.harvard.edu

to viruses and other invading pathogens<sup>12</sup>. TBK1 integrates upstream signals from pattern-recognition receptors and cytosolic nucleic acid sensors to regulate the activation of interferon regulatory factor 3 (IRF3) and consequent induction of type I interferons (IFN $\alpha$  and IFN $\beta$ ) and interferon-stimulated genes (ISGs) that are critical to the host immune response<sup>3</sup>. Activation of cytosolic nucleic-acid-sensing pathways has emerged as a promising strategy to stimulate innate anti-tumour immune responses to inflame immunologically ‘cold’ tumours<sup>13</sup>; it is therefore surprising that TBK1 has been nominated as a candidate immune-evasion gene<sup>4,9–11</sup> and that disrupting TBK1 signalling has shown early promise enhancing the response to ICB in mouse tumour models<sup>14,15</sup>. Given these seemingly contradictory findings, the precise role of TBK1 in influencing sensitivity to cancer immunotherapy remains unclear.

Here we show that genetic deletion of *TBK1* sensitizes tumours to immune attack and demonstrate that pharmacological inhibition of TBK1 can overcome resistance to PD-1 blockade using established mouse tumour models and patient-derived tumour models. Targeting TBK1 lowers the cytotoxicity threshold after exposure to immune-cell-derived effector cytokines, thereby sensitizing resistant tumours to ICB.

### TBK1 loss sensitizes tumours to ICB

In a previous in vivo CRISPR screen<sup>4</sup>, *Tbk1*-targeting single-guide RNAs (sgRNAs) were significantly depleted from B16 melanoma tumours in immunocompetent mice after PD-1 blockade (Fig. 1a), suggesting more effective tumour control of cells lacking TBK1. By contrast, the sgRNAs targeting the homologous innate immune signalling kinase IKK $\epsilon$  (*Ikkbe*) were not enriched (Extended Data Fig. 1a), suggesting specificity for TBK1. To determine whether the deletion of *Tbk1* enhanced the response to PD-1 blockade, we generated B16 mouse melanoma cells lacking *Tbk1* by CRISPR–Cas9 knockout using two different sgRNAs and confirmed the loss of TBK1 protein expression (Extended Data Fig. 1b). *Tbk1*-null and control sgRNA B16 cells grew at comparable rates in culture and when implanted into immunodeficient NOD.Cg-Prkdcscid1l2rgtm1Wjl/SzJ (NSG) mice (Fig. 1b and Extended Data Fig. 1c,d). Tumour growth and survival was comparable in immunocompetent wild-type (WT) mice bearing control and *Tbk1*-null B16 tumours, whereas anti-PD-1 treatment resulted in improved tumour shrinkage and increased survival in mice bearing *Tbk1*-null B16 tumours compared with mice bearing control sgRNA B16 tumours (Fig. 1c and Extended Data Fig. 1e). These results confirm that *Tbk1*-null B16 tumours demonstrate normal growth compared with control sgRNA B16 tumours and are more sensitive to cancer immunotherapy with PD-1 blockade in vivo.

### TBK1 inhibition enhances ICB response

TBK1 has an important role in innate immune sensing<sup>3</sup> and TBK1 inhibitors are being evaluated in the treatment of autoimmune and inflammatory diseases<sup>16</sup>. This raises the possibility that systemic inhibition of TBK1 may dampen inflammation and fail to recapitulate the sensitization mediated by tumour-specific TBK1 loss. Thus, we sought to determine whether pharmacological inhibition of TBK1 phenocopied the observations in TBK1-null B16 tumours. To this end, WT mice bearing B16 tumours expressing the model antigen ovalbumin (B16-ova) were treated with IgG or anti-PD-1 antibodies with or without a previously described small-molecule TBK1 inhibitor (TBK1i)<sup>14</sup>. Improved tumour control was observed in mice that were treated with anti-PD-1 plus TBK1i compared with mice that were treated with a single agent or the control mice (Fig. 1d and Extended Data Fig. 1f,g), and was well tolerated without evidence of toxicity or diminished body weight (Extended Data Fig. 1h). Ex vivo profiling using mouse-derived organotypic tumour spheroids (MDOTS)<sup>14</sup> derived from untreated mice bearing B16-ova tumours confirmed the enhanced response to anti-PD-1 plus TBK1i (Fig. 1e). Using CT26 MDOTS (partially responsive to PD-1 blockade with or without TBK1i)<sup>14</sup> with or

without anti-CD8 $\alpha$  treatment, we demonstrated that CD8 T cell activity was required for the combinatorial effect of anti-PD-1 plus TBK1i, but not single-agent TBK1i (Extended Data Fig. 1i). Ex vivo profiling of MDOTS derived from anti-PD-1-resistant D4M.3A (*Braf*-mutant/*Pten*-null) tumours<sup>17</sup> showed that TBK1i could overcome primary (intrinsic) resistance using a separate autochthonous mouse melanoma model (Fig. 1f). A similar sensitizing effect of TBK1i was observed in B16-ova MDOTS prepared from mice that developed acquired (secondary) resistance to PD-1 blockade in vivo (Fig. 1g). We also observed improved in vivo tumour control with combined TBK1i plus PD-1 blockade in MC38 (responsive) and MB49 (partially responsive) syngeneic mouse tumour models (Extended Data Fig. 1j,k). These findings demonstrate activity of TBK1i + anti-PD-1 in mouse tumour models of primary (intrinsic) and secondary (acquired) resistance to PD-1 blockade.

### TBK1i enhances ICB response in PDOTS

To examine TBK1 inhibition as a strategy to overcome intrinsic or acquired resistance to ICB in human cancer, we performed ex vivo profiling of patient-derived organotypic tumour spheroids (PDOTS)<sup>14,18</sup> from explanted human tumours (Fig. 2a). PDOTS established from patients with melanoma and other cancers were cultured ex vivo with TBK1i (1  $\mu$ M) with or without anti-PD-1. Analysis of PDOTS ( $n = 30$ ) from patients with cutaneous melanoma ( $n = 15$ ), non-cutaneous melanoma ( $n = 2$ ) and other cancer types ( $n = 13$ ) revealed reduced tumour growth in response to TBK1i (30% response) and TBK1i plus PD-1 blockade (40% response) compared with single-agent PD-1 blockade (16.6% response) (Fig. 2b, Extended Data Fig. 2a and Supplementary Table 1). We did not observe an effect of IgG4 antibody control (Extended Data Fig. 2b), consistent with previous reports<sup>14,19</sup>. PDOTS from patients with immunotherapy-resistant metastatic cutaneous melanoma were sensitive to combined TBK1i + anti-PD-1 treatment and were unresponsive to ex vivo anti-PD-1 with or without anti-CTLA-4 treatment (Fig. 2c,d). An exceptional ex vivo response to TBK1i + PD-1 blockade was also observed in other cancer types, especially colorectal carcinoma with evidence of microsatellite instability (MSI) (Fig. 2e,f). These data demonstrate the efficacy of a TBK1 inhibitor in combination with PD-1 blockade using patient-derived tumour models, including models derived from patients with clinical ICB resistance.

### TBK1i and the tumour immune landscape

TBK1 and IKK $\epsilon$  (encoded by *IKBKE*) are widely expressed across lymphoid and myeloid cells in human melanoma<sup>20</sup> (Extended Data Fig. 3a,b). Recent studies have demonstrated critical roles for TBK1 and/or IKK $\epsilon$  in regulating the activity of numerous immune cell types, including T cells<sup>21</sup>, B cells<sup>22,23</sup>, dendritic cells<sup>24</sup> and macrophages<sup>25,26</sup>. To examine the effect of TBK1 inhibition on the tumour immune microenvironment, we performed single-cell RNA-sequencing (scRNA-seq) analysis of CD45<sup>+</sup> cells ( $n = 53,637$ ) from B16-ova tumours from mice treated with anti-PD-1, TBK1i or anti-PD-1 plus TBK1i, compared with treatment with the isotype control (IgG) (Fig. 3a). We aggregated data from each treatment condition to perform clustering to create a stable set of clusters across conditions and then quantified changes in the relative abundance of populations between conditions (Fig. 3b and Extended Data Fig. 3b). As expected, treatment with anti-PD-1 expanded the populations of T and natural killer (NK) cells relative to the other treatment conditions (Fig. 3b and Extended Data Fig. 3c,d) with an increase in the proportion of terminal exhausted/effector CD8<sup>+</sup> T cells (Extended Data Fig. 3e–g). By contrast, tumours from mice treated with TBK1i with or without anti-PD-1 demonstrated enrichment in early exhausted/effector CD8<sup>+</sup> T cells with a concomitant reduction in the abundance of terminal exhausted/effector CD8<sup>+</sup> T cells (Extended Data Fig. 3f,g). In vitro treatment of T lymphocytes derived from mouse spleens with TBK1i enhanced the production of cytokines and tumour necrosis

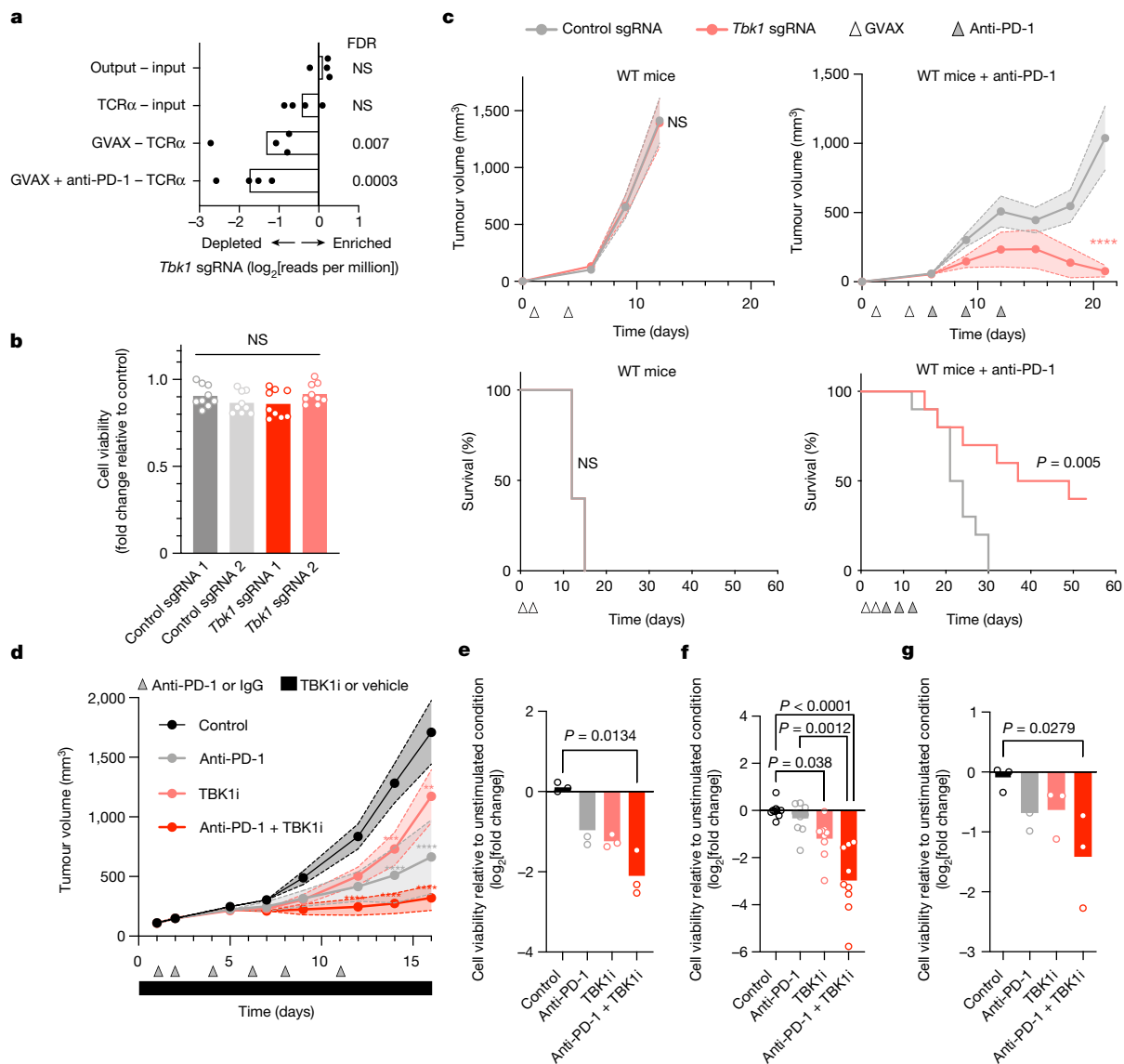


**Fig. 1** | TBK1 loss sensitizes tumours to PD-1 blockade. **a**, Relative depletion of *Tbk1* sgRNAs from a pool of sgRNAs targeting 2,368 genes expressed by Cas9-expressing B16 melanoma cells. *n* = 4 independent guides targeting each gene. False-discovery rate (FDR)-adjusted *P* values were calculated using the STARS algorithm v.1.3, as previously described<sup>6,7</sup>. **b**, The viability of *Tbk1*-null and control B16 tumour cells after 3 days of in vitro culture. Mean values (bars) and individual values (open circles) are shown. *n* = 9 biological replicates, across 3 independent experiments. Statistical analysis was performed using one-way analysis of variance (ANOVA) with Tukey’s multiple-comparison test. **c**, Tumour volume and survival analysis of control (grey) and *Tbk1*-null (light red) B16 tumours in WT and WT anti-PD-1-treated C57BL/6 mice with overlapping survival curves for granulocyte-macrophage colony-stimulating factor (GM-CSF)-secreting, irradiated tumour cell vaccine (GVAX)-treated WT mice. Data in **c** represent two independent experiments with *n* = 5 mice per guide with two

separate guides for the control group and two separate guides for each *Tbk1*-null group. Data are mean (solid circles) ± s.e.m. (shaded region) tumour volumes. **d**, Tumour volume analysis of mice bearing B16-ova tumours treated with TBK1i (compound 1, 40 mg per kg daily by oral gavage), anti-PD-1 (200 mg i.p. three times per week; × 6 doses) or a combination of both compared with the control (IgG + vehicle); *n* = 10 mice per treatment group. Data are mean (solid circles) ± s.e.m. (shaded region) tumour volumes. Statistical analysis was performed using two-way ANOVA with Tukey’s multiple-comparison test compared with the control group; \*\*\*\**P* < 0.001. **e–g**, Viability assessment of treatment-naïve B16-ova MDOTS (*n* = 3 per treatment group) (**e**), treatment-naïve *Braf/Pten* (D4M.3A) MDOTS (*n* = 9 per treatment group) (**f**) and anti-PD-1-resistant B16-ova MDOTS (*n* = 3 per treatment group) (**g**). Statistical analysis was performed using one-way ANOVA with Dunn’s multiple-comparison test. \**P* < 0.05, \*\**P* < 0.01, \*\*\**P* < 0.001, \*\*\*\**P* < 0.0001; NS, not significant.

factor (TNF), interleukin-2 (IL-2) and interferon- $\gamma$  (IFN $\gamma$ ) (Extended Data Fig. 3h–j), consistent with an enhanced effector function.

A marked expansion of myeloid cells was observed in tumours from mice treated with TBK1i with or without anti-PD-1 (Fig. 3b). Subclustering of tumour-infiltrating myeloid cells revealed a marked increase in the abundance of several pro-inflammatory macrophage populations (such as M1 macrophages) with a decreased abundance of certain immune suppressive myeloid populations, including myeloid-derived suppressor cells (MDSCs) (Fig. 3c–e). To gain additional insights into the effect

of TBK1i with or without anti-PD-1 treatment on immune cell function, gene set enrichment analysis was performed. TBK1i with or without anti-PD-1 treatment was associated with enrichment for numerous gene sets associated with TNF–NF- $\kappa$ B signalling and inflammation (Fig. 3f,g). TNF (*Tnf*) and IL-1 $\alpha$  (*Il1a*) expression was largely observed in myeloid cell clusters, and this was further enhanced in tumours from mice treated with TBK1i with or without anti-PD-1 (Fig. 3h,i). Pretreatment with TBK1i enhanced the expression of *Tnf* and *Il1a* in bone-marrow-derived macrophages in response to challenge with

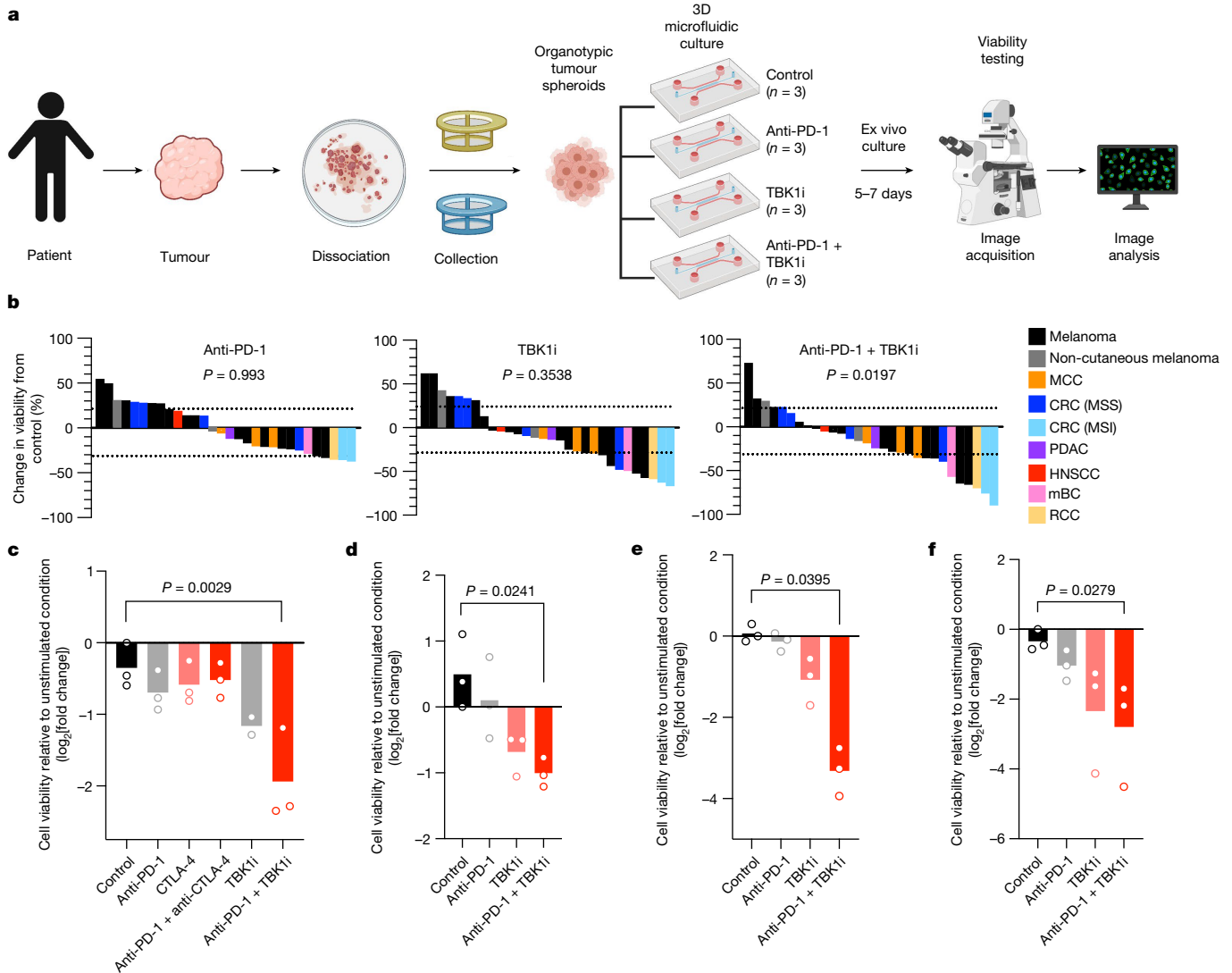


**Fig. 2 | TBK1 inhibition enhances sensitivity to PD-1 blockade using PDOTS.** **a**, Schematic of PDOTS preparation. The diagram was created using BioRender. **b**, Waterfall plots for PDOTS ( $n = 30$ , indicated tumour types) treated with anti-PD-1 (250  $\mu\text{g ml}^{-1}$  pembrolizumab), TBK1i (1  $\mu\text{M}$ ) or combined anti-PD-1 + TBK1i. Mean values (bars) for each sample are shown. Statistical analysis was performed using one-way ANOVA (matched) with Dunnett's multiple-comparison test compared with the control. MCC, Merkel cell carcinoma; CRC, colorectal cancer; MSS, microsatellite stable; PDAC, pancreatic ductal

adenocarcinoma; HNSCC, head and neck squamous cell carcinoma; mBC, metastatic breast cancer; RCC, renal cell carcinoma. **c–f**, PDOTS viability assessment from patients with anti-PD-1-refractory melanoma (PDOTS-01 (**c**) and PDOTS-06 (**d**)) and treatment-naive MSI-colon adenocarcinoma (CRC (MSI-H), PDOTS-04 (**e**) and CRC (MSI-H), PDOTS-07 (**f**)) with the indicated treatments. Mean values (bars) and individual values (open circles) are shown.  $n = 3$ , biological replicates. Statistical analysis was performed using one-way ANOVA with Dunn's multiple-comparison test.

lipopolysaccharide (LPS) and IFN $\gamma$  (Fig. 3j), confirming a direct effect of TBK1 inhibition on myeloid cell inflammatory responses. These findings demonstrate a tumour-extrinsic effect of TBK1i with marked remodelling of the myeloid compartment in response to TBK1i with or without anti-PD-1 treatment and confirm that TBK1i is sufficient to enhance the expression of inflammatory cytokines (such as IFN $\gamma$  and TNF) in the tumour microenvironment.

We next sought to determine whether tumour-specific loss of TBK1 influenced the tumour immune microenvironment. Flow cytometry analysis of tumour-infiltrating immune cells from control and *Tbk1*-null B16 tumours implanted into WT mice and treated with anti-PD-1 treatment revealed no significant differences in CD8 $^+$  or CD4 $^+$  T cells, granzyme B $^+$  CD8 $^+$  T cells, FOXP3 $^+$  regulatory T cells, NK cells or F4/80 $^+$  myeloid cells (Extended Data Fig. 4a). We next performed scRNA-seq analysis of CD45 $^+$  cells ( $n = 31,810$ ) from control and *Tbk1*-null B16 tumours after anti-PD-1 treatment and identified distinct lymphoid and myeloid cell clusters, as well as contaminating tumour cells (Extended

Data Fig. 4b). Evaluation of the immune cell states using scRNA-seq revealed limited immune remodelling in *Tbk1*-null B16 tumours with modest increases in CD8 $^+$  T cells and M1-like macrophages (Extended Data Fig. 4c,d). We confirmed the expression of *Tbk1* and *Ikbke* across lymphoid and myeloid cell types or states, with the highest expression in macrophages, MDSCs and CD8 $^+$  T cells (Extended Data Fig. 4e,f). As expected, we observed a loss of *Tbk1* expression in tumour cells from *Tbk1*-null B16 tumours with intact expression of *Ikbke* (Extended Data Fig. 4f). These findings confirm that the enhanced efficacy of anti-PD-1 therapy in mice bearing *Tbk1*-null tumours is not dependent on significant remodelling of the immune compartment, consistent with a tumour-intrinsic role for TBK1 as an immune evasion gene.

### Loss of TBK1 enhances sensitivity to TNF and IFN $\gamma$

IFN $\gamma$  and TNF are key effector cytokines that contribute to anti-tumour immune responses<sup>9,11,27–30</sup>, and genes associated with IFN and TNF

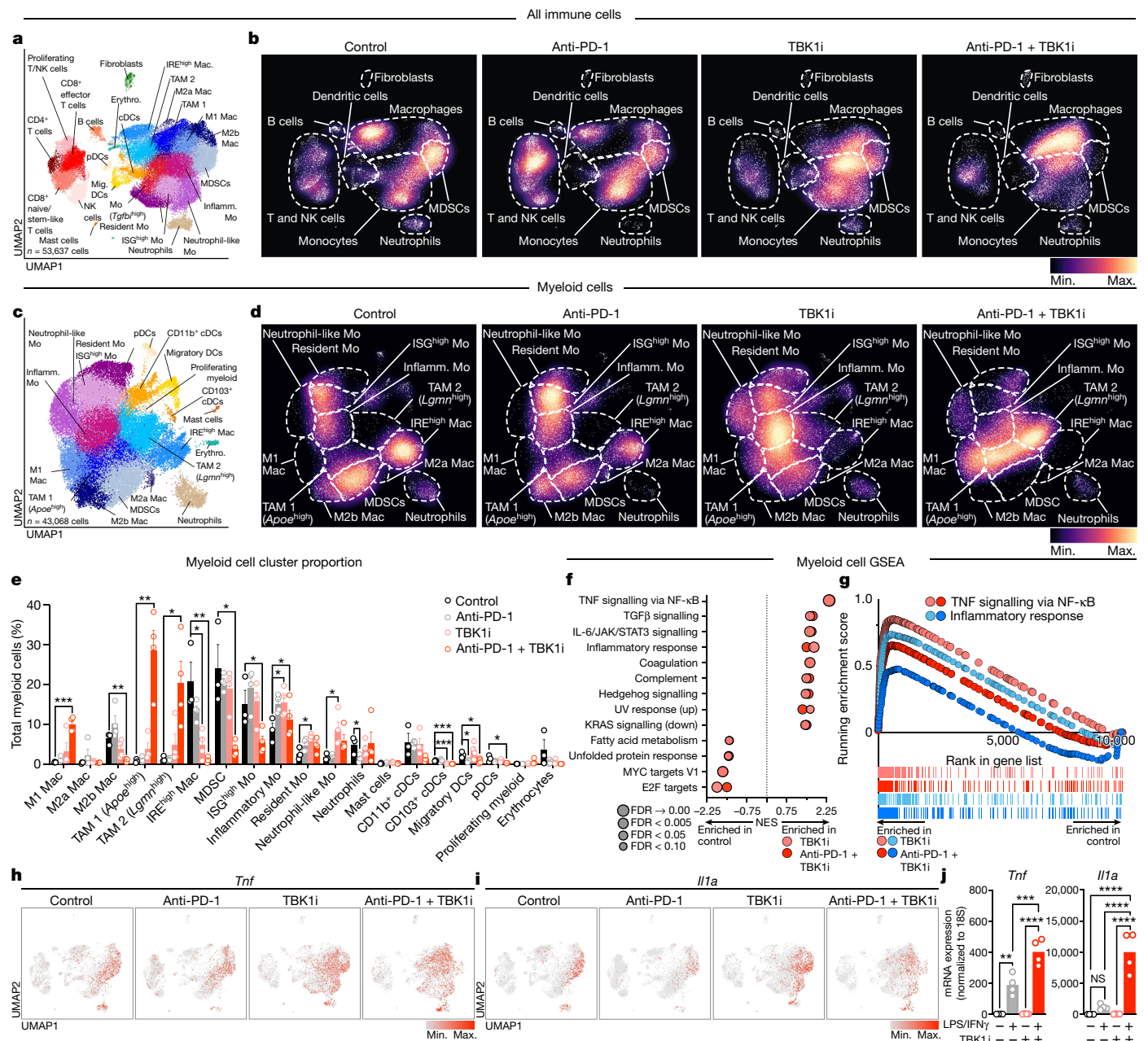


**Fig. 3 | TBK1 inhibition remodels the tumour immune microenvironment.** **a**, Uniform manifold approximation and projection (UMAP) analysis of all immune cells ( $n = 53,637$ ) with 25 unique populations identified among CD45<sup>+</sup>-enriched immune cells from scRNA-seq analysis of tumour-infiltrating leukocytes from B16-ova tumours from control (vehicle/IgG,  $n = 3$ ) and anti-PD-1-treated (vehicle/anti-PD-1,  $n = 4$ ), TBK1i-treated (TBK1i/IgG,  $n = 4$ ) and anti-PD-1 + TBK1i-treated (TBK1i/anti-PD-1,  $n = 4$ ) tumours. cDCs, conventional dendritic cells; Erythro., erythrocytes; Inflamm., inflammatory; Mac, macrophages; Mig., migrating; Mo, monocytes; pDCs, plasmacytoid dendritic cells; TAM, tumour-associated macrophages. **b**, Downsampled cell density projections by condition. **c**, UMAP analysis of 43,068 cells and 19 unique populations identified among subclustered myeloid cells. **d**, Downsampled myeloid subcluster cell density projections by condition. **e**, The proportional changes by unique cluster of myeloid subcluster immune cells by treatment. Data are mean  $\pm$  s.e.m. with individual values (circles).  $n = 4$  biologically independent samples, except

for the control, for which  $n = 3$ . Statistical analysis was performed using multiple unpaired  $t$ -tests. **f**, The top enriched or decreased Hallmark gene signatures in the myeloid subcluster determined by GSEA preranked on differentially expressed genes calculated by a logistic regression by condition. NES, normalized enrichment score. **g**, Mountain plots showing enrichment scores for TNF signalling through the NF- $\kappa$ B Hallmark gene set and inflammatory response gene set in the myeloid subcluster by condition. **h, i**, Downsampling UMAP analysis of all immune cells showing *Tnf* gene expression (**h**) and *Il1a* gene expression (**i**) by condition. **j**, Gene expression analysis (RT-qPCR) of *Tnf* and *Il1a* in bone-marrow-derived macrophages that were pretreated with TBK1i (1  $\mu$ M) for 24 h before stimulation for 2 h stimulation with LPS (20 ng ml<sup>-1</sup>) plus IFN $\gamma$  (20 ng ml<sup>-1</sup>) versus PBS control. Mean values (bars) and individual values (open circles) are shown.  $n = 4$  biological replicates. Statistical analysis was performed using two-way ANOVA with Sidak's multiple-comparison test.

signalling pathways contribute to immune evasion<sup>4,9,29</sup>. In a cohort of 203 patients with metastatic melanoma, elevated circulating levels of TNF and IFN $\gamma$  were observed in both responsive and non-responsive patients 6 weeks after initiating ICB treatment, although the levels

remained elevated at 6 months in non-responsive patients (Fig. 4a,b). scRNA-seq data from patients with melanoma treated with ICB<sup>20</sup> confirmed higher expression of *IFNG* and *TNF* in non-responsive versus responsive tumours (Fig. 4c). Expression of *IFNG* was largely restricted

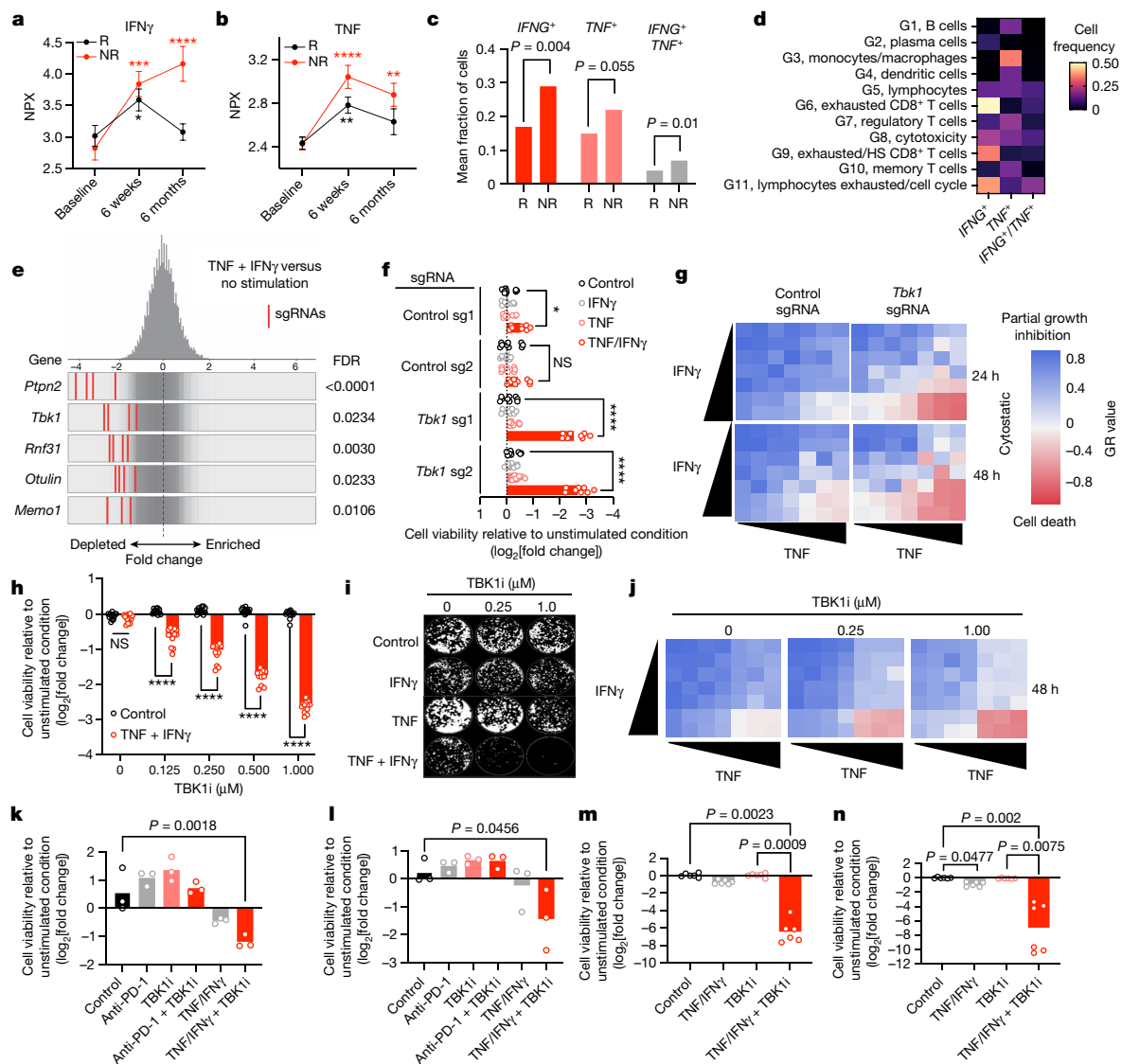


**Fig. 4 | Loss of TBK1 sensitizes tumour cells to TNF/IFN $\gamma$ .** **a, b**, Plasma IFN $\gamma$  (**a**) and TNF (**b**) protein levels (normalized protein expression (NPX)) from patients with metastatic melanoma responsive (R) or non-responsive (NR) to ICB at baseline ( $n = 179$ ), 6 weeks after starting ICB ( $n = 173$ ) and 6 months after starting ICB ( $n = 151$ ). Data are mean  $\pm$  s.e.m. Statistical analysis was performed using two-way ANOVA with Dunnett's multiple-comparison test. **c, d**, The mean fraction of CD45 $^{+}$  cells (**c**) and cell frequency across lineage-defined clusters (**d**) for cells expressing *IFNG* and *TNF* in patients with metastatic melanoma<sup>20</sup>. **e**, Frequency histograms of depletion (Z-score) for all sgRNAs per target in a Cas9 $^{+}$  B16 control sgRNA cell line with or without in vitro stimulation with TNF and IFN $\gamma$ . **f**, Viability assessment of the indicated B16 cell lines with the indicated treatments (24 h). Mean values (bars) and individual values (open circles) are shown.  $n = 9$  biological replicates, 3 independent experiments. Statistical analysis was performed using two-way ANOVA with Dunnett's multiple-comparison test. **g**, Mean GR values ( $n = 3$  biological replicates) for cells treated

with increasing concentrations of TNF and IFN $\gamma$ . **h**, Viability assessment of B16 cells with the indicated treatments compared with unstimulated cells (24 h). Mean values (bars) and individual values (open circles) are shown.  $n = 12$ , 4 independent experiments. Statistical analysis was performed using two-way ANOVA with Dunnett's multiple-comparison test. **i**, Clonogenic assay of B16 cells. Representative images are shown.  $n = 3$ . **j**, GR values for B16 cells treated with TBK1i ( $n = 3$ ) across TNF/IFN $\gamma$  concentrations. **k, l**, Viability assessment of anti-PD-1-refractory cutaneous melanoma (PDOTS-24; **k**) and ocular melanoma (PDOTS-10; **l**) after the indicated treatments. Mean values (bars) and individual values (open circles) are shown.  $n = 3$ . Statistical analysis was performed using one-way ANOVA with Dunn's multiple-comparison test. **m, n**, Viability of CRC (MSI-H) (PDO-04; **m**) and CRC (MSI-H) (PDO-07; **n**) after the indicated treatments. Mean values (bars) and individual values (open circles) are shown.  $n = 6$  biological replicates, 2 independent experiments. Statistical analysis was performed using one-way ANOVA with Dunn's multiple-comparison test.

to the lymphoid compartment (highest expression in exhausted CD8 T cells), whereas *TNF* expression was enriched in macrophages and monocytes (Fig. 4d), consistent with the findings in B16 tumours (Extended Data Fig. 5a). Importantly, levels of *Tnf* and *Ifng* were similar across immune, stromal and tumour cell populations from control and *Tbk1*-null B16 tumours (Extended Data Fig. 5b). These results confirm the upregulation of TNF and IFN $\gamma$  after ICB and demonstrate persistent cytokine elaboration in patients who are not responding to therapy.

Given the limited remodelling of the immune compartment in *Tbk1*-null B16 tumours and comparable expression of effector cytokines, we reasoned that B16 cells lacking TBK1 exhibited increased sensitivity to TNF and IFN $\gamma$ . In a whole-genome in vitro pooled CRISPR screen, *Tbk1* was among the top depleted sgRNAs in cells challenged with the combination of TNF and IFN $\gamma$  (hereafter, TNF/IFN $\gamma$ ) (Fig. 4e and Extended Data Fig. 6a), consistent with in vivo CRISPR screening findings in B16 melanoma tumours<sup>6</sup> (Fig. 1a). In vitro essentiality analysis confirmed that *Tbk1* is not an essential gene (Extended Data

Fig. 6b), consistent with our initial findings on the in vitro (Fig. 1b and Extended Data Fig. 1b) and in vivo (Fig. 1c and Extended Data Fig. 1c) growth characteristics of *Tbk1*-null B16 melanoma cells. *Tbk1*-null B16 cells exhibited marked sensitivity to combined TNF/IFN $\gamma$  treatment, but not with either cytokine alone (Fig. 4f). Using single-cell clones, we demonstrate that the response to TNF/IFN $\gamma$  was influenced by the extent of *Tbk1* deletion, with a considerable reduction in cell viability in clones 3 and 4 (complete loss of TBK1 expression), whereas no effect was observed in clone 2 (intact TBK1 expression) and a partial response was observed in clone 1 (with or without TBK1 expression) (Extended Data Fig. 6c,d). Normalized growth rate inhibition (GR) analysis<sup>31</sup> across a range of both IFN $\gamma$  and TNF concentrations revealed partial growth inhibition with TNF/IFN $\gamma$  treatment in control B16 cells, whereas a marked cytotoxic response was observed exclusively in *Tbk1*-null B16 cells above threshold concentrations of TNF and IFN $\gamma$  (Fig. 4g).

### TBK1i promotes TNF/IFN $\gamma$ cytotoxicity

To determine the effect of pharmacological TBK1 inhibition on cell viability, parental B16 cells were treated with increasing concentrations of TBK1i with or without TNF/IFN $\gamma$ . TBK1i alone had no effect on the cell viability at the doses evaluated (up to 1.0  $\mu$ M), whereas TBK1i in combination with TNF/IFN $\gamma$  reduced cell viability in a dose-dependent manner in B16 cells (Fig. 4h). TBK1i also prevented B16 colony formation in the presence of TNF/IFN $\gamma$  and, to a lesser extent, with TNF alone (Fig. 4i). The activity of TBK1i in the presence of TNF/IFN $\gamma$  was confirmed using B16-ova cells (Extended Data Fig. 6a) and parental B16 tumour spheroids in 3D culture (Extended Data Fig. 6b). Comparable findings in B16 cells were observed using two additional TBK1 inhibitors—MRT67307<sup>32</sup> and GSK8612<sup>33</sup> (Extended Data Fig. 6g,h) and the TBK1-targeted proteolysis targeting chimera (TBK1 PROTAC 3i)<sup>34</sup> (Extended Data Fig. 6i).

GR analysis confirmed a dose-dependent effect of TBK1i in parental B16 melanoma cells at concentrations of TNF and IFN $\gamma$  required to induce cytotoxicity in *Tbk1*-null B16 cells (Fig. 4j). Dose–response studies demonstrated that TBK1i (up to 1.0  $\mu$ M) with or without IFN $\gamma$  or TNF alone did not affect growth or viability of control or *Tbk1*-null B16 cells, whereas TBK1i induced a dose-dependent cytotoxic response in cells that were cotreated with combined TNF/IFN $\gamma$ , mirroring the cytotoxic response observed in *Tbk1*-null B16 cells treated with TNF/IFN $\gamma$  (Extended Data Fig. 7a). Further GR analysis of B16 cells confirmed enhanced TBK1i potency (half-maximal effect (GEC<sub>50</sub>)) and overall efficacy (area over the GR curve (GR<sub>AOC</sub>)) in cells treated with TNF/IFN $\gamma$  (Extended Data Fig. 7b,c).

To confirm these findings in other model systems, we examined tumour-cell-intrinsic sensitivity to TNF/IFN $\gamma$  using human melanoma cell lines, PDOTS and patient-derived organoids (PDOs). Similar to B16 cells, TBK1i sensitized A375 human melanoma cells to TNF/IFN $\gamma$  in a time- and dose-dependent manner (Extended Data Fig. 7d). Notably, A375 cells with acquired resistance to combined BRAF and MEK inhibition exhibited increased sensitivity to TBK1i compared with parental A375 cells (Extended Data Fig. 7e). Evaluation of PDOTS, including anti-PD-1 refractory cutaneous melanoma (Fig. 4k) and ocular melanoma (Fig. 4l), demonstrated that tumours that are poorly responsive to ICB could be sensitized to exogenous TNF/IFN $\gamma$  by co-administration of TBK1i. Finally, matched PDOs from exceptional ex vivo responders to combined TBK1i + anti-PD-1 treatment (PDOTS-04 and PDOTS-07; Fig. 2e,f and Extended Data Fig. 2) demonstrated notable sensitivity to TBK1i + TNF/IFN $\gamma$  (Fig. 4m,n). These results show in human and mouse melanoma cell lines, as well as in patient-derived tumour models including PDOTS and PDOs, that TBK1i treatment lowers the cytotoxic threshold to TNF/IFN $\gamma$ .

### TBK1 restrains necroptosis

TBK1 restrains cell death signalling downstream of the TNF receptor (TNFR)<sup>35,36</sup> by phosphorylating receptor-interacting protein kinase

1 (RIPK1). Loss of TBK1 reduces this inhibitory phosphorylation, thereby promoting RIPK1 activation leading to enhanced TNFR complex II formation and subsequent caspase 8 cleavage and activation<sup>35</sup>. To determine the effect of TBK1 loss on RIPK1 activation and caspase cleavage, we performed an immunoblot analysis of cell lysates from control and *Tbk1*-null B16 cells treated with TNF/IFN $\gamma$ . Increased levels of phosphorylated RIPK1 (p-RIPK1, Ser166/Thr189) were observed in *Tbk1*-null B16 cells within 3 h of TNF/IFN $\gamma$  treatment, which preceded cleavage of caspase 8, caspase 3 and PARP, and c-FLIP degradation (Fig. 5a). To assess the requirement for RIPK and caspase signalling in response to TNF/IFN $\gamma$ , control and *Tbk1*-null B16 cells were pretreated with Nec-1s (RIPK1 inhibitor) and/or zDEVD-fmk (caspase 3 inhibitor). Nec-1s and zDEVD-fmk each partially prevented the loss of cell viability in *Tbk1*-null B16 cells after TNF/IFN $\gamma$  challenge, whereas combined RIPK1 and caspase 3 inhibitor was necessary to completely prevent cell death (Fig. 5b). Similar findings were observed using pan-caspase inhibitors (Q-VD-OPH and zVAD-fmk), and a caspase-8-selective inhibitor (z-IETD-fmk) (Extended Data Fig. 8a–c).

Necroptosis is a form of death that is regulated by RIPK1 involving downstream activation of RIPK3 and the pseudokinase mixed-lineage domain-like (MLKL)<sup>37</sup>. Consistent with our findings with RIPK1, treatment with small-molecule inhibitors of RIPK3 (HS-1371)<sup>38</sup> or MLKL (GW806742X)<sup>39</sup> rescued *Tbk1*-null B16 cells from TNF/IFN $\gamma$ -induced cell death when combined with caspase inhibition (Extended Data Fig. 8d,e). Inhibition of RIPK1, RIPK3 or MLKL also rescued parental B16 cells from cell death after treatment with TBK1i plus TNF/IFN $\gamma$  in a clonogenic assay (Extended Data Fig. 8f–h). Transcriptional upregulation of MLKL was observed in response to IFN $\gamma$  with or without TNF (Extended Data Fig. 8i), consistent with previous reports<sup>40</sup>. Upregulation of MLKL expression was also more pronounced in *Tbk1*-null B16 cells after TNF/IFN $\gamma$  (Extended Data Fig. 8j). In addition to pRIPK1 and cleavage of caspase 8 and caspase 3, increased phosphorylated (Ser358) and total MLKL was also observed in *Tbk1*-null B16 cells after TNF/IFN $\gamma$  treatment (Extended Data Fig. 8k), which was reversed with RIPK1 with or without caspase inhibition.

Consistent with a primary role for TBK1 in regulating necroptosis after TNF/IFN $\gamma$  treatment, *Tbk1*-null B16 cells did not exhibit baseline or induced differences in apoptotic priming, compared with control sgRNA B16 cells. BCL2-homology domain (BH3) profiling<sup>41</sup> demonstrated that cytochrome c release after mitochondrial exposure to pro-apoptotic BH3-only peptides (such as BIM BH3 and PUMA BH3) was similar in control and *Tbk1*-null B16 cells (Extended Data Fig. 9a). After TNF/IFN $\gamma$  treatment, the effect of TBK1 loss on apoptotic priming was also modest, with the most marked shifts driven by the differential response to TNF/IFN $\gamma$  treatment in *Tbk1*-null B16 cells (Extended Data Fig. 9b). Consistent with these findings, control and *Tbk1*-null B16 cells exhibited identical sensitivity to the apoptosis-inducing pan-kinase inhibitor staurosporine in 2D and 3D culture (Extended Data Fig. 9c,d). In summary, loss of TBK1 did not fundamentally alter apoptotic priming or sensitivity to cytotoxic agents, whereas melanoma cells lacking TBK1 were more sensitive to RIPK- and caspase-dependent cell death after TNF/IFN $\gamma$  challenge.

### STING is dispensable for necroptosis

TBK1 has a central role in coordinating the innate immune response in response to cytosolic nucleic acids (for example, the CGAS–STING–TBK1–IRF3–IFN type I pathway)<sup>3</sup>, and enhanced sensitivity to TNF has been shown to drive the CGAS–STING-dependent interferon response and effect cell viability<sup>42</sup>. To evaluate the role of the STING–TBK1–IRF3 axis, we generated B16 cells in which *Sting1* (also known as *Tmem173*) and *Irf3* were deleted with or without *Tbk1* deletion (Extended Data Fig. 9e,f). B16 cells lacking *Tmem173* and *Irf3* did not exhibit enhanced sensitivity to combined TNF/IFN $\gamma$  challenge (Extended Data Fig. 9g), and co-deletion of *Tmem173* or *Irf3* with *Tbk1* did not alter sensitivity to

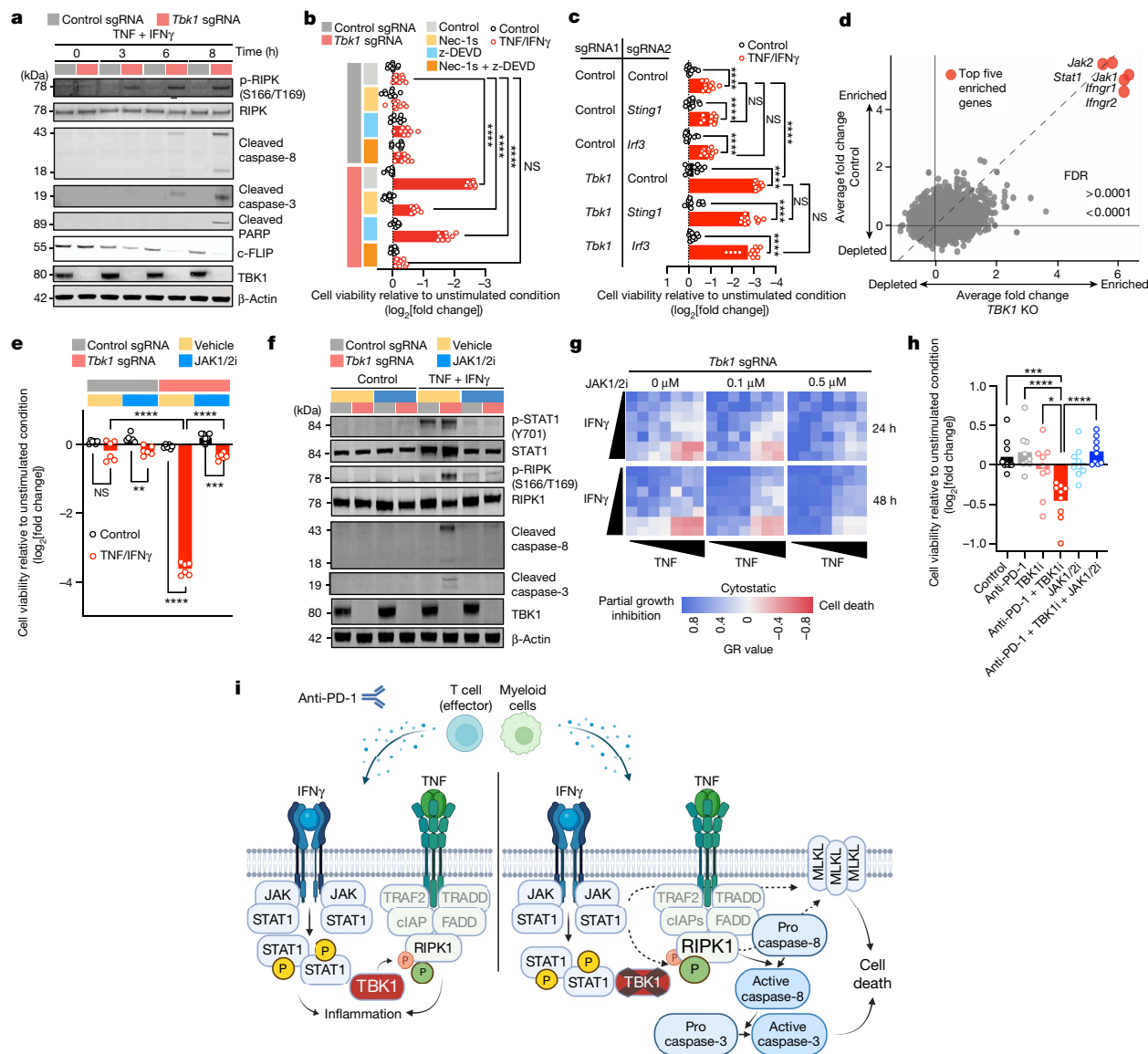


**Fig. 5 | IFN $\gamma$  sensing is required for RIPK- and caspase-dependent death of *Tbk1*-null cells.** **a**, Western blot analysis of the indicated proteins in control sgRNA and *Tbk1*-null B16 cells treated with TNF (160 ng ml<sup>-1</sup>) and IFN $\gamma$  (40 ng ml<sup>-1</sup>) for the indicated times. **b**, Viability assessment of control and *Tbk1*-null B16 cells with the indicated pretreatments with or without TNF and IFN $\gamma$ . Mean values (bars) and individual values (open circles) are shown.  $n = 9$  biological replicates, 3 independent experiments. Statistical analysis was performed using two-way ANOVA with Dunnett's multiple-comparison test. **c**, Viability assessment of the indicated B16 cells after 48 h treatment with TNF and IFN $\gamma$  compared with unstimulated cells. Mean values (bars) and individual values (open circles) are shown.  $n = 8$  biological replicates, 2 independent experiments. Statistical analysis was performed using two-way ANOVA with Tukey's multiple-comparison test. **d**, The relative depletion and enrichment of sgRNAs targeting 19,674 genes in a Cas9<sup>+</sup> B16 control and *Tbk1* sgRNA cell line with or without in vitro stimulation with TNF and IFN $\gamma$ . **e**, Cell viability assessment of the

indicated B16 cells that were pretreated with ruxolitinib (0.5  $\mu$ M) with or without TNF/IFN $\gamma$ . Mean values (bars) and individual values (open circles) are shown.  $n = 6$  biological replicates, 2 independent experiments. Statistical analysis was performed using two-way ANOVA with Dunnett's multiple-comparison test. **f**, Western blot analysis of the indicated proteins in control sgRNA and *Tbk1*-null B16 cells that were pretreated with vehicle or ruxolitinib (0.5  $\mu$ M) followed by TNF/IFN $\gamma$  or PBS (control) for 8 h. **g**, Mean GR values ( $n = 3$  biological replicates) for *Tbk1*-null B16 cells treated with increasing concentrations of TNF and IFN $\gamma$  for 24 and 48 h with 0, 0.1 and 0.5  $\mu$ M ruxolitinib. **h**, Viability assessment of melanoma PDOTS with the indicated treatments. Mean values (bars) and individual values (open circles) are shown.  $n = 9$  biological replicates, 3 independent specimens. Statistical analysis was performed using one-way ANOVA with Dunn's multiple-comparison test. **i**, Schematic of TNF/IFN $\gamma$ -driven RIPK1- and caspase-dependent cell death in cells lacking TBK1. The diagram was created using BioRender.

TNF/IFN $\gamma$  (Fig. 5c). Finally, treatment of melanoma PDOTS with a STING agonist (ADU-S100<sup>43,44</sup>) had no effect on PDOTS viability, in contrast to TNF/IFN $\gamma$  with or without TBK1i (Extended Data Fig. 9h). To confirm activity of the STING agonist in PDOTS, we performed multiplexed analysis of secreted cytokines and observed upregulation of several inflammatory cytokines and chemokines (for example, CXCL10) after treatment with ADU-S100 (Extended Data Fig. 9i). Together with the observation of aberrant RIPK1 activation in cells lacking TBK1, these

findings indicate the TNF/IFN $\gamma$ -driven death of *Tbk1*-null cells occurs independently of cytosolic nucleic acid sensing pathways (that is, the STING–TBK1–IRF3 axis).

### Requirement for intact IFN $\gamma$ sensing

To uncover genes and/or pathways that are required for sensitivity of *Tbk1*-null cells to TNF/IFN $\gamma$ , we performed a whole-genome pooled

in vitro CRISPR screen using both control sgRNA and *Tbk1* sgRNA B16 cells. sgRNAs targeting genes involved in IFN $\gamma$  sensing (*Ifngr1*, *Ifngr2*, *Jak1*, *Jak2* and *Stat1*) were enriched in control and *Tbk1*-null cells (Fig. 5d and Extended Data Fig. 10a), consistent with previous in vivo and in vitro screens<sup>4,29</sup>. By contrast, sgRNAs targeting key components of the TNFR and necroptosis signalling pathways (for example, *Ripk1*, *Ripk3*, *Birc2*, *Birc3* and *Casp8*) were not significantly enriched (or depleted) in either control sgRNA or *Tbk1*-null B16 cells (Extended Data Fig. 10b), possibly reflecting the greater complexity of cell death signalling downstream of the TNF receptor. Notably, no differences were observed in the activation of IFN-sensing pathways (for example, JAK1–JAK2–STAT1), NF- $\kappa$ B (p65) or IRF3 between control and *Tbk1*-null B16 cells (Extended Data Fig. 10c). Pretreatment with ruxolitinib (JAK1 and JAK2 inhibitor) completely rescued *Tbk1*-null B16 cells and TBK1i-treated parental B16 cells from TNF/IFN $\gamma$ -mediated cell death (Fig. 5e and Extended Data Fig. 10d). In addition to completely blocking STAT1 phosphorylation (Tyr701) in both control and *Tbk1*-null B16 cells, ruxolitinib pretreatment abolished RIPK1 phosphorylation (Ser166/Thr169), caspase 8 cleavage and caspase 3 cleavage in *Tbk1*-null B16 cells (Fig. 5f and Extended Data Fig. 10e). GR analysis confirmed that ruxolitinib restored the viability of *Tbk1*-null B16 cells by converting the cytotoxic response into a cytostatic response, mirroring the response characteristics of parental and control sgRNA B16 cells (Fig. 5g and Extended Data Fig. 10f). Finally, we observed that JAK1 and JAK2 inhibition rescued melanoma PDOTS treated with anti-PD-1 plus TBK1i (Fig. 5h). These data confirm that enhanced sensitivity to TNF/IFN $\gamma$  in B16 cells lacking TBK1 requires IFN sensing and provide a link between IFN $\gamma$ -induced JAK–STAT signalling and TNF-mediated RIPK1 activation (Fig. 5i).

## Discussion

Here we show that *TBK1* is an immune-evasion gene and that targeting TBK1 can enhance the response to PD-1 blockade by sensitizing tumour cells to effector-cytokine-induced cell death. Using syngeneic mouse tumour models and patient-derived ex vivo models, we demonstrate that targeting TBK1 sensitizes tumours to immune challenge. In contrast to other recently characterized immune-evasion genes<sup>4,8,45</sup>, tumour-specific loss of TBK1 did not result in substantial remodelling of the immune compartment. Rather, TBK1 loss sensitized tumour cells to immune-cell-derived effector cytokines (TNF and IFN $\gamma$ ), a finding confirmed in an independent, whole-genome in vitro CRISPR screen and subsequent validation studies. Whereas a key role for TNF signalling has been demonstrated in immunotherapy-resistant melanoma cell lines devoid of IFN $\gamma$  signalling<sup>11</sup>, our findings demonstrate critical interplay between TNF and IFN $\gamma$  signalling that can be taken advantage of therapeutically to sensitize tumour cells to immune attack.

Despite multiple loss-of-function CRISPR screens (in vivo and in vitro) identifying *TBK1* as a potential immune-evasion gene<sup>4,9–11</sup>, the finding that TBK1 inhibition can enhance the response to cancer immunotherapy is surprising. Intact TBK1 signalling is required for response to STING agonists, innate immune stimulatory molecules that mimic response to cytosolic DNA, which have been shown to limit tumour growth alone or in combination with cancer immunotherapy<sup>46–48</sup>. However, TBK1 has an emerging role in regulating death receptor signalling distinct from its role in innate immune response and viral sensing<sup>35,36,49</sup>. Here we demonstrate that the loss of TBK1 leads to RIPK- and caspase-dependent cell death after challenge with TNF and IFN $\gamma$ , and confirm that STING and IRF3 are dispensable for this tumour-intrinsic cell death phenotype.

Although the loss of TBK1 signalling did not affect tumour growth in immunodeficient mice or in isolated cancer cell lines, moderate anti-tumour activity was observed after pharmacological inhibition of TBK1 in models containing tumour cells and autologous immune cells, suggesting a tumour-extrinsic effect of TBK1 inhibition. Consistent with these observations, treatment with TBK1i increased the proportion of

early exhausted/effector CD8 T cells and M1 macrophages in the tumour immune microenvironment, and enhanced the expression or production of effector cytokines in vitro using isolated CD8 T cells and macrophages. Thus, TBK1i treatment not only lowered the cytotoxic threshold of tumour cells to TNF and IFN $\gamma$ , but also promoted elaboration of TNF and IFN $\gamma$  from tumour-infiltrating immune cells. Although marked systemic upregulation of TNF and IFN $\gamma$  can promote tissue damage<sup>50</sup>, observations from patients with inherited TBK1 deficiency suggests that the loss of TBK1 signalling is associated with a milder TNF-driven autoinflammatory syndrome, but not sepsis or increased incidence or severity of viral illnesses<sup>49</sup>. Importantly, treatment of mice with TBK1i with or without anti-PD-1 did not result in weight loss or other signs of systemic toxicity. Future studies will be required to further deconvolute the roles of TBK1 in distinct immune cell populations and determine the therapeutic potential of disrupting TBK1 signalling in patients with melanoma that is resistant to immunotherapy.

Two central challenges in the field of cancer immunotherapy are (1) the need for preclinical models that translate to human immunity and (2) strategies to effectively and efficiently assess cancer immunotherapy combinations<sup>51</sup>. With over 1,000 cancer immunotherapy combination trials under evaluation<sup>5</sup>, new approaches are needed to deprioritize ineffective treatment strategies and to better understand mechanisms of response and resistance to new therapeutic strategies. Mouse models are amenable to in vivo, ex vivo and in vitro manipulation and iterative experimentation, but lack the heterogeneity observed in human cancer. Patient-derived models are inherently heterogeneous and more complex but offer greater clinical relevance and enable the evaluation of the distribution of treatment response across multiple patients using clinically relevant biospecimens. Our results not only support further evaluation and development of TBK1-directed therapeutic strategies, but also provide a framework to evaluate potential immune evasion targets across multiple model systems using a combination of genetic and pharmacological tools.

## Online content

Any methods, additional references, Nature Portfolio reporting summaries, source data, extended data, supplementary information, acknowledgements, peer review information; details of author contributions and competing interests; and statements of data and code availability are available at <https://doi.org/10.1038/s41586-023-05704-6>.

- Jenkins, R. W., Barbie, D. A. & Flaherty, K. T. Mechanisms of resistance to immune checkpoint inhibitors. *Br. J. Cancer* **118**, 9–16 (2018).
- Sharma, P., Hu-Lieskovan, S., Wargo, J. A. & Ribas, A. Primary, adaptive, and acquired resistance to cancer immunotherapy. *Cell* **168**, 707–723 (2017).
- Zhou, R., Zhang, Q. & Xu, P. TBK1, a central kinase in innate immune sensing of nucleic acids and beyond. *Acta Biochim. Biophys. Sin.* **52**, 757–767 (2020).
- Manguso, R. T. et al. In vivo CRISPR screening identifies Ptpn2 as a cancer immunotherapy target. *Nature* **547**, 413–418 (2017).
- Tang, J., Shalabi, A. & Hubbard-Lucey, V. M. Comprehensive analysis of the clinical immuno-oncology landscape. *Ann. Oncol.* **29**, 84–91 (2018).
- Gogas, H. et al. Cobimetinib plus atezolizumab in BRAF<sup>V600</sup> wild-type melanoma: primary results from the randomized phase III ImSpire170 study. *Ann. Oncol.* **32**, 384–394 (2021).
- Long, G. V. et al. Epcadostat plus pembrolizumab versus placebo plus pembrolizumab in patients with unresectable or metastatic melanoma (ECHO-301/KEYNOTE-252): a phase 3, randomised, double-blind study. *Lancet Oncol.* **20**, 1083–1097 (2019).
- Ishizuka, J. J. et al. Loss of ADAR1 in tumours overcomes resistance to immune checkpoint blockade. *Nature* **565**, 43–48 (2019).
- Lawson, K. A. et al. Functional genomic landscape of cancer-intrinsic evasion of killing by T cells. *Nature* **586**, 120–126 (2020).
- Pan, D. et al. A major chromatin regulator determines resistance of tumor cells to T cell-mediated killing. *Science* **359**, 770–775 (2018).
- Vredevoogd, D. W. et al. Augmenting immunotherapy impact by lowering tumor TNF cytotoxicity threshold. *Cell* **178**, 585–599 (2019).
- Zhao, C. & Zhao, W. TANK-binding kinase 1 as a novel therapeutic target for viral diseases. *Expert Opin. Ther. Targets* **23**, 437–446 (2019).
- Kwon, J. & Bakhroum, S. F. The cytosolic DNA-sensing cGAS-STING pathway in cancer. *Cancer Discov.* **10**, 26–39 (2020).
- Jenkins, R. W. et al. Ex vivo profiling of PD-1 blockade using organotypic tumor spheroids. *Cancer Discov.* **8**, 196–215 (2018).

15. Zhu, L. et al. TBKBP1 and TBK1 form a growth factor signalling axis mediating immunosuppression and tumourigenesis. *Nat. Cell Biol.* **21**, 1604–1614 (2019).
16. Hasan, M. & Yan, N. Therapeutic potential of targeting TBK1 in autoimmune diseases and interferonopathies. *Pharmacol. Res.* **111**, 336–342 (2016).
17. Lo, J. A. et al. Epitope spreading toward wild-type melanocyte-lineage antigens rescues suboptimal immune checkpoint blockade responses. *Sci. Transl. Med.* **13**, eabd8636 (2021).
18. Aref, A. R. et al. 3D microfluidic ex vivo culture of organotypic tumor spheroids to model immune checkpoint blockade. *Lab Chip* **18**, 3129–3143 (2018).
19. Voabil, P. et al. An ex vivo tumor fragment platform to dissect response to PD-1 blockade in cancer. *Nat. Med.* **27**, 1250–1261 (2021).
20. Sade-Feldman, M. et al. Defining T cell states associated with response to checkpoint immunotherapy in melanoma. *Cell* **175**, 998–1013 (2018).
21. Yu, J. et al. Regulation of T-cell activation and migration by the kinase TBK1 during neuroinflammation. *Nat. Commun.* **6**, 6074 (2015).
22. Lee, M. S. J. et al. B cell-intrinsic TBK1 is essential for germinal center formation during infection and vaccination in mice. *J. Exp. Med.* **219**, e20211336 (2022).
23. Jin, J. et al. The kinase TBK1 controls IgA class switching by negatively regulating noncanonical NF- $\kappa$ B signaling. *Nat. Immunol.* **13**, 1101–1109 (2012).
24. Xiao, Y. et al. The kinase TBK1 functions in dendritic cells to regulate T cell homeostasis, autoimmunity, and antitumor immunity. *J. Exp. Med.* **214**, 1493–1507 (2017).
25. Gao, T. et al. Myeloid cell TBK1 restricts inflammatory responses. *Proc. Natl Acad. Sci. USA* **119**, e2107742119 (2022).
26. Hagan, R. S., Torres-Castillo, J. & Doerschuk, C. M. Myeloid TBK1 signaling contributes to the immune response to influenza. *Am. J. Respir. Cell Mol. Biol.* **60**, 335–345 (2019).
27. Barth Jr, R. J., Mule, J. J., Spiess, P. J. & Rosenberg, S. A. Interferon gamma and tumor necrosis factor have a role in tumor regressions mediated by murine CD8<sup>+</sup> tumor-infiltrating lymphocytes. *J. Exp. Med.* **173**, 647–658 (1991).
28. Benci, J. L. et al. Tumor interferon signaling regulates a multigenic resistance program to immune checkpoint blockade. *Cell* **167**, 1540–1554 (2016).
29. Kearney, C. J. et al. Tumor immune evasion arises through loss of TNF sensitivity. *Sci. Immunol.* **3**, eaar3451 (2018).
30. Kearney, C. J. et al. PD-L1 and IAPs co-operate to protect tumors from cytotoxic lymphocyte-derived TNF. *Cell Death Differ.* **24**, 1705–1716 (2017).
31. Hafner, M., Niepel, M., Chung, M. & Sorger, P. K. Growth rate inhibition metrics correct for confounders in measuring sensitivity to cancer drugs. *Nat. Methods* **13**, 521–527 (2016).
32. Clark, K. et al. Novel cross-talk within the IKK family controls innate immunity. *Biochem. J.* **434**, 93–104 (2011).
33. Thomson, D. W. et al. Discovery of GSK8612, a highly selective and potent TBK1 inhibitor. *ACS Med. Chem. Lett.* **10**, 780–785 (2019).
34. Crew, A. P. et al. Identification and characterization of Von Hippel-Lindau-recruiting proteolysis targeting chimeras (PROTACs) of TANK-binding kinase 1. *J. Med. Chem.* **61**, 583–598 (2018).
35. Lafont, E. et al. TBK1 and IKK $\epsilon$  prevent TNF-induced cell death by RIPK1 phosphorylation. *Nat. Cell Biol.* **20**, 1389–1399 (2018).
36. Xu, D. et al. TBK1 suppresses RIPK1-driven apoptosis and inflammation during development and in aging. *Cell* **174**, 1477–1491 (2018).
37. Weinlich, R., Oberst, A., Beere, H. M. & Green, D. R. Necroptosis in development, inflammation and disease. *Nat. Rev. Mol. Cell Biol.* **18**, 127–136 (2017).
38. Park, H.-H. et al. HS-1371, a novel kinase inhibitor of RIP3-mediated necroptosis. *Exp. Mol. Med.* **50**, 1–15 (2018).
39. Hildebrand, J. M. et al. Activation of the pseudokinase MLKL unleashes the four-helix bundle domain to induce membrane localization and necroptotic cell death. *Proc. Natl Acad. Sci. USA* **111**, 15072–15077 (2014).
40. Knuth, A.-K. et al. Interferons transcriptionally up-regulate MLKL expression in cancer cells. *Neoplasia* **21**, 74–81 (2019).
41. Montero, J. et al. Drug-induced death signaling strategy rapidly predicts cancer response to chemotherapy. *Cell* **160**, 977–989 (2015).
42. Heijink, A. M. et al. BRCA2 deficiency instigates cGAS-mediated inflammatory signaling and confers sensitivity to tumor necrosis factor- $\alpha$ -mediated cytotoxicity. *Nat. Commun.* **10**, 100 (2019).
43. Sivick, K. E. et al. Magnitude of therapeutic sting activation determines CD8 T cell-mediated anti-tumor immunity. *Cell Rep.* **29**, 785–789 (2019).
44. Knelson, E. H. et al. Activation of tumor-cell STING primes NK-cell therapy. *Cancer Immunol. Res.* **10**, 947–961 (2022).
45. Griffin, G. K. et al. Epigenetic silencing by SETDB1 suppresses tumour intrinsic immunogenicity. *Nature* **595**, 309–314 (2021).
46. Zhu, Y. et al. STING: a master regulator in the cancer-immunity cycle. *Mol. Cancer* **18**, 152 (2019).
47. Wang, H. et al. cGAS is essential for the antitumor effect of immune checkpoint blockade. *Proc. Natl Acad. Sci. USA* **114**, 1637–1642 (2017).
48. Woo, S. R. et al. STING-dependent cytosolic DNA sensing mediates innate immune recognition of immunogenic tumors. *Immunity* **41**, 830–842 (2014).
49. Taft, J. et al. Human TBK1 deficiency leads to autoinflammation driven by TNF-induced cell death. *Cell* **184**, 4447–4463 (2021).
50. Karki, R. et al. Synergism of TNF- $\alpha$  and IFN- $\gamma$  triggers inflammatory cell death, tissue damage, and mortality in SARS-CoV-2 infection and cytokine shock syndromes. *Cell* **184**, 149–168 (2021).
51. Hegde, P. S. & Chen, D. S. Top 10 challenges in cancer immunotherapy. *Immunity* **52**, 17–35 (2020).

**Publisher's note** Springer Nature remains neutral with regard to jurisdictional claims in published maps and institutional affiliations.

Springer Nature or its licensor (e.g. a society or other partner) holds exclusive rights to this article under a publishing agreement with the author(s) or other rightsholder(s); author self-archiving of the accepted manuscript version of this article is solely governed by the terms of such publishing agreement and applicable law.

© The Author(s), under exclusive licence to Springer Nature Limited 2023

## Methods

### Generation of CRISPR-edited tumour cell lines

For in vivo and in vitro validation experiments, confirmatory epistasis experiments, *Tbk1* was deleted in B16 cells using transient transfection of a Cas9-sgRNA plasmid (pX459, Addgene) with Lipofectamine 3000 (Thermo Fisher Scientific, L3000015) followed by puromycin selection. For epistasis experiments, Cas9 was expressed using the pLX311 backbone, transient transfection was used to introduce the first guide(s), and the final epistasis guides were expressed using the pXPR\_BRD024 lentiviral expression system. Cell lines were tested every 3–6 months for mycoplasma contamination.

### Animal treatment and tumour challenges

The designs of animal studies and procedures were approved by the Broad Institute, Massachusetts General Hospital and Charles River Laboratories IACUC committees. Ethical compliance with IACUC protocols and institute standards was maintained. Specific-pathogen-free facilities at the Broad Institute were used for the storage and care of all mice. Mouse pathogen testing and mycoplasma testing was performed before tumour inoculations. WT female C57BL/6J mice (aged 7 weeks) were obtained from Jackson Laboratories. A colony of NOD.Cg-Prkdcscid Il2rgtm1Wjl/SzJ (NSG) mice were bred on site at the Broad Institute. Mice were age-matched to be 6–12 weeks old at the time of tumour inoculation. For tumour challenges,  $2.0 \times 10^6$  B16 tumour cells were resuspended in Hanks balanced salt solution (Gibco), mixed 1:1 by volume with Matrigel (Corning) and subcutaneously injected into the right flank on day 0. Each tumour injected contained only a single sgRNA targeting each indicated gene or control sgRNA. Vaccination on days 1 and 4 with  $1.0 \times 10^6$  previously irradiated GM-CSF-secreting B16 (GVAX) cells (provided by G. Dranoff) was performed where indicated. For validation experiments, mice were treated with 200 µg of rat monoclonal anti-PD1 antibodies (BP0273, BioXCell, 29F.1A12) through intraperitoneal injection on days 6, 9 and 12. Beginning on day 6 after challenge, tumour volumes were estimated using longest dimension (length) and the longest perpendicular dimension (width), using the formula  $(L \times W^2)/2$ . Tumour volumes were assessed every 3–4 days until either the survival end point was reached, or no palpable tumour remained. Prespecified end points for tumour size were adhered to as defined by IACUC protocols, including 2.0 cm in maximum dimension for validation studies and 2.5 cm in maximum dimension for screens with daily monitoring. CO<sub>2</sub> inhalation was used to euthanize mice. Statistical methods were not used to predetermine sample size. At least five mice were included in each group for all of the experiments. Mice were randomized before treatment. No blinding was performed.

TBK1i in vivo studies were performed by Charles River Laboratories. For TBK1i in vivo treatment studies, WT female C57BL/6J mice (aged 7–8 weeks) were obtained from Charles River Laboratories. A total of  $1.0 \times 10^6$  B16-ova cells (provided by D. Sen) were resuspended in sterile Ca- and Mg-free PBS (Gibco), mixed 1:1 by volume with Matrigel (Corning) and subcutaneously injected into the flank on day 0. The mice were randomized into four groups of ten using the stratified method in the Studylog program on the basis of tumour size. Randomization and treatment initiated on day 1; the mean tumour volume at the start of dosing was 110.05 mm<sup>3</sup>. Vehicle (0.5% hydroxypropyl methylcellulose K100LV, 0.4% Tween-80, 99.1% 0.05 N hydrochloric acid) or TBK1i (compound 1, Gilead Sciences; 40 mg per kg)<sup>14</sup> was administered by oral gavage daily (days 1–18) and isotype control IgG (BE0089, 2A3, BioXCell) or anti-PD-1 (BP0273, BioXCell, 29F.1A12) (10 mg per kg) was administered three times weekly for a total of six doses. Investigators were not blinded to treatment groups. Combination studies using the MC38 and MB49 models were performed by vivoPharm. MB49 cells (used for in vivo studies only) were licensed from K. Esuvaranathan by vivoPharm in collaboration with Gilead Sciences. All of the procedures

used in the performance of these studies were performed in accordance with vivoPharm's standard operating procedures, with particular reference to US\_SOPvP\_EF0314 'General Procedures for Efficacy Studies'. Vehicle and TBK1i (40 mg per kg) were administered by oral gavage daily for 26 days and isotype control or a reverse chimera anti-PD-L1 cloned from literature reports and placed into a mouse IgG1 framework (10 mg per kg)<sup>52</sup> was administered every 5 days for a total of six doses. Investigators were not blinded to the treatment groups.

For the MDOTS studies, mice were euthanized 8–14 days after inoculation and tumours were collected. B16 and B16-ova MDOTS were prepared from tumours using WT female C57BL/6J mice (aged 6 weeks, Jackson Labs). D4M.3A (*Braf/Pten*) MDOTS were generated using WT male C57BL/6J mice (aged 6 weeks, Jackson Labs). CT26 MDOTS were prepared using WT female BALB/c mice (aged 6–8 weeks, Jackson Labs).

### Isolation and culture of primary mouse T cells

Spleens collected from C57BL/6J mice were mechanically dissociated, filtered through a 70-µm filter and incubated in 1 ml ACK lysing buffer per spleen for 1 min. Cells were quenched in 10× the lysis buffer volume with a PBS + 2% FBS + 5 mM EDTA solution. T cells were isolated using the mouse CD8a<sup>+</sup> T Cell Isolation Kit (Miltenyi Biotec) according to the manufacturer's instructions. T cells were cultured on a plate coated with purified NA/LE hamster anti-mouse CD3e antibodies and in T/NK cell medium supplemented with 1 µg ml<sup>-1</sup> purified NA/LE hamster anti-mouse CD28 antibodies, 100 U ml<sup>-1</sup> rhIL-2, and either 1 µM TBK1i (compound 1) or an equal volume of DMSO. After incubation for 24 h, T cells were centrifuged out of their medium to remove the CD3e and CD28 antibodies and transferred to ultralow-attachment plates. Cells were cultured in T/NK medium supplemented with rhIL-2 and either 1 µM TBK1i (compound 1) or an equal volume of DMSO for an additional 96 h with a 50% medium volume refresh every 48 h. On the sixth day after isolation, T cells were pooled by TBK1i treatment status, replated at a final concentration of  $2 \times 10^6$  cells per ml and stimulated with ionomycin (0.5 µg ml<sup>-1</sup>, Millipore Sigma, I0634) and PMA (5 ng ml<sup>-1</sup>, Millipore Sigma, P8139). After stimulation for 2 h, brefeldin A (1×, Invitrogen/eBioscience) was added to the culture medium. Cells were incubated for an additional 2 h before collection for analysis using flow cytometry.

### Analysis of primary mouse T cells using flow cytometry

Cells were stained with conjugated fluorescent monoclonal antibodies against CD69 (104527, H1.2F3, BioLegend) and CD25 (102024, PC61, BioLegend). After washing, cells were fixed and permeabilized using the BD Cytofix/Cytoperm Fixation/Permeabilization kit (BD Biosciences) according to the manufacturer's instructions. Cells were stained with conjugated fluorescent monoclonal antibodies against IFNγ (505807, XMGL2, BioLegend), TNF (506303, MP6-XT22, BioLegend) and IL-2 (503821, JES6-5H4, BioLegend). All of the samples were acquired on the Beckman Coulter Cytoflex LX flow cytometry system using single-colour compensation controls to set gate margins and analysed with FlowJo software (FlowJo).

### Isolation, culture and stimulation of bone-marrow-derived macrophages

Mouse bone-marrow-derived macrophages (BMDMs) were generated by flushing bone marrow from the bones of the hind legs (day 0) and differentiated to macrophages by culturing for 7 days in 12-well plates ( $2 \times 10^6$  cells per well) in DMEM with 10% FCS plus M-CSF (20 ng ml<sup>-1</sup>, vendor details) with medium exchange and fresh M-CSF added on day 4 and day 6. On day 8, the medium was exchanged with fresh M-CSF with TBK1i (1 µM) or DMSO (0.1%) for 24 h. On day 9, LPS (20 ng ml<sup>-1</sup>, Sigma-Aldrich, L4391) and IFNγ (20 ng ml<sup>-1</sup>, PeproTech, 315-05) or vehicle control (PBS) were added. After 2 h, medium was aspirated from dishes and cells were collected in RNeasy lysis buffer for subsequent RT-qPCR analysis.

### Analysis of tumour-infiltrating immune cells using flow cytometry

*Tbkl*-null (sgRNA-1) or control sgRNA-1 B16 tumour cells ( $2 \times 10^6$ ) were implanted in Matrigel into abdominal subcutaneous tissue of C57BL/6 female mice. On day 13, tumours were dissected from the surrounding fascia, mechanically minced and dissociated using the mouse Tumor Dissociation Kit (Miltenyi Biotec) according to the manufacturer's instructions. After filtering through a 70- $\mu$ m filter, live cells were isolated using a gradient with Lympholyte-M separation medium (Thermo Fisher Scientific) according to the manufacturer's instructions. Tumour-infiltrating lymphocytes were enriched by CD45<sup>+</sup> MACS positive selection (Miltenyi Biotec). Cells were then stained with conjugated fluorescent monoclonal antibodies against CD45 (103139, 30-F11, BioLegend), F4/80 (157306, QA17A29, BioLegend), CD8 $\alpha$  (100749, 53-6.7, BioLegend), CD4 (100538, RM4-5, BioLegend), NK1.1 (404-5941-82, PK136, Invitrogen) and TCR $\beta$  (109220, H57-597, BioLegend). After washing, cells were fixed and permeabilized using the FoxP3/Transcription Factor Staining Buffer Set (eBiosciences) according to the manufacturer's instructions. Cells were stained with conjugated fluorescent monoclonal antibodies against FOXP3 (12-5773-82, FJK-16s, Invitrogen) and granzyme B (515403, GB11, BioLegend). All of the samples were acquired using the Beckman Coulter Cytoflex instrument and analysed using FlowJo (FlowJo).

### Analysis of tumour-infiltrating immune cells by scRNA-seq

For TBK1  $\pm$  anti-PD-1 studies, subcutaneous B16-ova tumours were implanted into C57BL/6J mice and treated with control IgG or anti-PD-1 therapy in the presence of either vehicle or TBK1i as described above. Tumours were dissected on day 14 after inoculation and disassociated using the Miltenyi Mouse Tumor Dissociation Kit and gentleMACS Octo-Dissociator (Miltenyi) using the m-TKD-1 program. After filtering through a 70- $\mu$ m filter, live cells were isolated using a density gradient with Lympholyte-M separation medium (Cedarlane Labs) according to the manufacturer's specifications. CD45<sup>+</sup> tumour-infiltrating immune cells were enriched by positive selection with MicroBeads (Miltenyi) and a magnetic separator (Miltenyi). Four representative samples from each of the control (vehicle/IgG-treated), anti-PD-1 (vehicle/anti-PD-1-treated), TBK1i (TBK1i/IgG-treated) and anti-PD-1 + TBK1i groups were selected and droplet-based isolation of single cells was performed using the Chromium Controller (10x Genomics) according to the manufacturer's specifications. Subsequent generation of 3' sequencing libraries was performed according to the manufacturer's instructions (10x Genomics). Libraries were prepared using the Chromium Next GEM Single Cell Reagent Kits 3' v2 chemistry (10x Genomics). Characterization of the sequencing library was performed using the TapeStation (Agilent) and Qubit (Thermo Fisher Scientific) instruments.

Pooled equimolar 3' 10x output libraries were sequenced using two Illumina SP flow cells and two paired-end 150 bp cycle kits. Downstream preprocessing steps were performed using Cell Ranger (v.5.0.1). Individual replicate quality was evaluated on the basis of the number of cells recovered, mean reads per cell and median genes per cell. Before preprocessing, filtering or sample exclusion, 106,949 cells were recovered across all conditions. Early quality-control metrics determined that a single sample from the control (vehicle/IgG-treated) arm should be excluded on the basis of a low capture rate of CD45<sup>+</sup> cells. Additional cell and gene filtering was performed using Scanpy (v.1.7.2)<sup>53</sup>. Cells with greater than 10% mitochondrial gene content were excluded. Cells with more than 2,500 genes were excluded as suspected doublets, whereas cells that had less than 500 genes were excluded owing to poor gene capture. Moreover, genes that were not recovered in any cell were also excluded from the downstream analysis. Downstream analysis revealed unequal capture of contaminating B16OVA tumour cells (*Ptprc*<sup>+</sup>, *Mlana*<sup>+</sup>, *Mitf*<sup>+</sup> and *Dcn*<sup>+</sup>) across treatment conditions so suspected tumour cells were also excluded. Gene counts were library-size

normalized to 100,000 and log-transformed with a pseudocount of 1. Principal component analysis and nearest neighbour graphs were calculated to visualize on a UMAP plot. Harmony batch correction was then used to correct principal component analysis (PCA) embeddings for technical batch effects between experiments<sup>54</sup>. Cells were then grouped into 26 distinct clusters using the Leiden algorithm. Clusters driven by a high doublet score or markers of low cell viability, such as long non-coding RNAs, were excluded. After this additional filtering, 53,637 immune (*Ptprc*<sup>+</sup>) cells were left for downstream analysis. Cells were reclustered and classified on the basis of the built-in scanpy function one-versus-rest differential expression and immune-related gene signatures. To gain more granularity between the myeloid cell subtypes and T and NK cell subtypes, subclustering was performed on cells in specific clusters with specific marker gene expression profiles (clusters of cells expressing *Itgam*, *Itgax* and *Itgae* transcripts or on clusters of cells expressing *Cd8a*, *Cd4* and *Ncr1* transcripts, respectively). New PCA embeddings, nearest neighbourhood graphs and harmony batch corrections were calculated for this subgroup on a set of 10,000 highly variable genes. Differentially expressed genes between treatment conditions were calculated using a logistic regression model<sup>55</sup>. Ranked lists of differential genes were created using signed *P* values calculated by the logistic regression model and passed to GSEA Prerank to search for enriched gene sets by treatment<sup>56</sup>.

For tumour-specific TBK1 CRISPR studies, *Tbkl*-null (sgRNA 2) or control sgRNA-1 B16 tumour cells ( $2 \times 10^6$ ) were implanted in Matrigel into the stomach of C57BL/6 female mice. On day 13, tumours were dissected from the surrounding fascia, mechanically minced and dissociated using the Mouse Tumor Dissociation Kit (Miltenyi Biotec) according to the manufacturer's instructions. After filtering through a 70- $\mu$ m filter, live cells were isolated using a gradient with Lympholyte-M separation medium (Thermo Fisher Scientific) according to the manufacturer's instructions. Tumour-infiltrating immune cells were enriched by CD45<sup>+</sup> MACS positive selection (Miltenyi Biotec). Four representative samples each of *Tbkl*-null (sgRNA-1) or control sgRNA-1 samples were selected, counted and loaded onto the Chromium Controller (10x Genomics). Subsequent generation of 3' sequencing libraries was performed according to the manufacturer's instructions (10x Genomics). Characterization of the sequencing library was performed using the TapeStation (Agilent) and Qubit (Thermo Fisher Scientific) instruments. Pooled equimolar 3' 10x libraries were sequenced using the Illumina NextSeq 500 instrument with paired-end 50 bp reads. Sample demultiplexing, barcode processing and alignment was performed using the Cell Ranger analysis pipeline (v.3.0). Downstream analysis was performed using Scanpy (v.1.4.5post3). For each cell, two quality control metrics were calculated: (1) the total number of genes detected and (2) the proportion of unique molecular identifiers contributed by mitochondrially encoded transcripts. Cells in which fewer than 200 or greater than 2,500 genes were detected, or in which mitochondrially encoded transcripts constituted more than 10% of the total library, were excluded from downstream analysis. Tumour replicates were concatenated, and batch effect correction was performed using ComBat, implemented in Scanpy. The resulting expression matrix consisted of 34,223 cells by 31,053 genes. PCA dimensionality reduction was applied, and the first 50 principal components were used for UMAP projection into two-dimensional space. The Leiden algorithm was used to perform unsupervised clustering, and clusters were labelled by expression of canonical marker genes. For differential expression, between-cell normalization was calculated using scran (v.1.14.6), and the expression matrix was subset to genes expressed in at least 0.1% of cells, a total of 19,780 genes. Differential expression was then performed by logistic regression.

### Patient samples

Tumour samples were collected and analysed according to Dana-Farber/Harvard Cancer Center IRB-approved protocols. Informed consent was

# Article

obtained from all individuals. A cohort of patients (Supplementary Table 1) treated at Massachusetts General Hospital and the Dana-Farber Cancer Institute was assembled for PDOTS profiling. These studies were conducted according to the Declaration of Helsinki and approved by the DF/HCC IRB. Response to treatment was determined radiographically, as previously described<sup>14</sup>.

## Organotypic tumour spheroid preparation and microfluidic culture

MDOTS and PDOTS were prepared and cultured as previously described<sup>14</sup>. In brief, fresh tumour samples received in medium (DMEM or RPMI) on ice were minced in a standard 10 cm dish using sterile forceps and scalpel. Minced tumours were resuspended in high-glucose DMEM (RPMI for CT26) supplemented with 10% FBS + 1% penicillin–streptomycin and 100 U ml<sup>-1</sup> type IV collagenase and 15 mM HEPES (Life Technologies). After 15–30 min, equal volumes of medium were added to minced tumour samples. Cell suspensions were then pelleted and resuspended in fresh medium and passed over 100- $\mu$ m and 40- $\mu$ m filters sequentially to obtain the S1 (>100  $\mu$ m), S2 (40–100  $\mu$ m) and S3 (<40  $\mu$ m) spheroid fractions, which were subsequently transferred to ultralow-attachment tissue culture plates. The S2 fraction was pelleted and resuspended in type I rat tail collagen (Corning) at a concentration of 2.5 mg ml<sup>-1</sup> after the addition of 10 $\times$  PBS with phenol red with pH adjusted using NaOH. PANPEHA Whatman paper (Sigma-Aldrich) was used to confirm pH 7.0–7.5. The spheroid–collagen mixture was injected into the centre gel region of the AIM Dax-01 (AIM Biotech, Singapore) 3D microfluidic culture device (10  $\mu$ l per device). After incubation for 30 min at 37 °C in sterile humidity chambers, collagen hydrogels containing MDOTS/PDOTS were hydrated with medium with or without the indicated treatments: untreated control, anti-PD-1 (250  $\mu$ g ml<sup>-1</sup> pembrolizumab), TBK1i (1  $\mu$ M) or combined anti-PD-1 + TBK1i. Control human IgG4 (Invivogen, anti- $\beta$ -gal-hlgG4 (bgal-mab114), 100  $\mu$ g ml<sup>-1</sup>) was used for the indicated experiments

## Viability assessment of MDOTS/PDOTS

Dual-label fluorescence live/dead staining was using acridine orange/propidium iodide (AO/PI) staining solution (Nexcelom, CS2-0106) or Hoechst/propidium iodide (Ho/PI) staining solution (Nexcelom, CSK-V0005) as previously described<sup>14,18</sup>. After incubation with AO/PI (20 min, room temperature, protected from light) or Ho/PI (45 min, 37 °C, 5% CO<sub>2</sub>), images were obtained. Image capture and analysis are performed using a Nikon Eclipse NiE fluorescence microscope equipped with Z-stack (Prior), motorized stage (ProScan) and ZYLA5.5 sCMOS Camera (Andor) and NIS-Elements AR software package. Live and dead cell quantification was performed by measuring the total cell area of each dye. The percentage change and L2FC data were generated using raw fluorescence data (live) for given treatments relative to the control conditions.

## In vitro CRISPR screen

B16 cells (control and *Tbkl1*-null) expressing Cas9 (pLoxp311 cas9) were transduced with a library of lentiviral vectors encoding 78,637 sgRNAs targeting 19,674 genes in the mouse genome (Brie pXPR003, CP0044)<sup>57</sup> at >100 $\times$  coverage per sgRNA. Cells were selected and passaged in vitro for 8 days to allow sufficient time for gene editing. Subsequently, cells were stimulated with mouse TNF and IFN $\gamma$  (10 ng ml<sup>-1</sup>, each) or vehicle control (PBS) for 12 days. Subsequently, cell pellets were lysed in ATL buffer (QIAGEN) with proteinase K (QIAGEN) before genomic DNA extraction (QIAGEN Blood Maxi kit). DNA (120  $\mu$ g per sample condition) was PCR-amplified and sequenced using the Illumina HiSeq system. Significantly depleted or enriched sgRNAs were identified using the STARS algorithm, as previously described<sup>4,58</sup>. Gene essentiality analysis was conducted by calculating the log-transformed fold changes between sgRNAs at day 12 and day 0 for both the *TBKL1*-knockout condition and the control condition.

## In vitro cytokine stimulations and growth inhibition assays

Parental and CRISPR-edited B16.F10 tumour cells were plated in DMEM + 10% FBS containing the indicated combinations of cytokines. For cell growth and viability assays, 8,000 cells were plated in 96-well plates and viable cells were enumerated after 24 or 48 h using Cell Titer-Glo (Promega, G7570) after treatment mouse IFN $\gamma$  (40 ng ml<sup>-1</sup>, R&D Systems), mouse TNF (160 ng ml<sup>-1</sup>, R&D Systems). For inhibitor studies, B16 cells were pretreated for 2 h with the indicated doses of TBK1i (compound 1, Gilead Sciences)<sup>14</sup>, MRT67307 (MedChemExpress, HY-13018), GSK8612 (MedChemExpress, HY-111941), TBK1 PROTAC 3i (Bio-technique/TOCRIS, 7259), Nec-1s (MedChemExpress, HY-15760), HS-1371 (MedchemExpress, HY-114349), GW806742X (MedchemExpress, HY-112292A), Z-DEVD-fmk (R&D Systems, 2163/1), zVAD-FMK (R&D Systems, 2166/1), Q-VD-OPh (MedChemExpress, HY-12305), zIETD-FMK (R&D Systems, FMK007), staurosporine (APEXbio, A8192), birinapant (APEXbio, A4219), ADU-S100 (MedchemExpress, CT-ADUS100) and ruxolitinib (MedChemExpress, HY-50856). All of the compounds were dissolved in DMSO (0.1% final concentration), except for ADU-S100, which was dissolved in sterile water. The plates were read on a Cytation 5 plate reader and analysis was performed using Prism9 (GraphPad Software). All of the conditions were tested in triplicate. The values represent the average of three replicates and a representative experiment from at least two independent experiments.

## Normalized growth rate inhibition measurements

Cell lines, maintained in their recommended growth conditions were seeded depending on cell line and growth rate, in 384-well CellCarrier plates (Perkin Elmer) using a Multidrop Combi Reagent Dispenser (Thermo Fisher Scientific) and allowed to adhere to for 24 h before drug treatment. B16 cells were plated at 750 cells per well for the 24- and 48-h time points; and A375 (ATCC) and BRAFi/MEKi-resistant A375 cells (provided by G. Zhang)<sup>59</sup> were plated at 1,000 cells per well for the 24-, 48- and 72-h time points. Cells were treated with a half-log dilution series of TNF (R&D Systems, 0.005–500 ng ml<sup>-1</sup>) and IFN $\gamma$  (R&D Systems 0.001–125 ng ml<sup>-1</sup>) in combination by HP D300e Digital Dispenser (HP). Cytokines were prepared in PBS containing 0.05% Tween-20 (necessary for dispensing aqueous solutions), which was diluted to a final concentration of <0.0008% Tween-20 after addition to the wells. In conditions that included TBK1i, cells were pretreated for 2 h with the TBK1i (compound 1, Gilead Sciences<sup>14</sup>) at various concentrations before the addition of cytokines, which were all dispensed by the HP D300e Digital Dispenser. Cells were stained and fixed for analysis at the time of drug delivery and after 24, 48 and 72 h of treatment. Cells were stained with LIVE/DEAD Far Red Dead Cell Stain (LDR, 1:5,000) (Thermo Fisher Scientific) and 1  $\mu$ g ml<sup>-1</sup> Hoechst 33342 (Sigma-Aldrich). Cells were then fixed with 4% formaldehyde (Sigma-Aldrich) for 30 min. Fixed cells were imaged with a  $\times$ 10 objective using the ImageXpress confocal microscope (Molecular Devices). MetaXpress software was used to segment nuclei on the basis of their Hoechst signal, and the LDR intensity within each nuclear mask was extracted and used to classify cells as live or dead. Live-cell counts were normalized to DMSO-treated controls on the same plates to yield normalized GR values as described previously<sup>24</sup>. Experiments were performed in technical duplicate or triplicate unless otherwise indicated. The GR values shown in the heat maps depict the mean across three biological replicates.

## Clonogenic assay

A total of 500 B16.F10 cells were plated onto 6-well type plates, and then cultured in the presence of TBK1i (compound 1: 0, 0.25 or 1.0  $\mu$ M), Nec-1s (10  $\mu$ M), Q-VD-OPh (20  $\mu$ M), HS-1371 (2  $\mu$ M) or MLKL inhibitor GW806742X (2  $\mu$ M) in the presence of TNF (10 ng ml<sup>-1</sup>), IFN $\gamma$  (10 ng ml<sup>-1</sup>) or combined TNF + IFN $\gamma$  for 9 days. The medium was changed every 3 days with the indicated drugs. After 9 days of culture, cells were fixed with 4% paraformaldehyde, and then stained with 0.5% crystal violet

solution (20% methanol + 0.5% crystal violet). After washing excessive dye, crystal violet was extracted by using 10% acetic acid for 20 min incubation with shaking, diluted in water as necessary and images captured using the LiCOR Odyssey (fluorescence at 590 nm) converted to grey scale with colour inversion for final visualization.

### PDO generation, culture and viability assessment

Tumour specimens were minced and dissociated in S-MEM medium (Gibco) supplemented with Liberase (1:20, Sigma-Aldrich) on a heater-shaker (37 °C, 45 min), followed by resuspending and pelleting dissociated cells twice in DMEM/F12 supplemented with 10% FBS, 1% penicillin–streptomycin and 1% glutamate. Organoids were generated and cultured as previously described<sup>60</sup>. In brief, dissociated cells were seeded onto a 24-well plate in Matrigel and cultured in basal organoid growth medium (30% DMEM/F12 supplemented with 20% FBS, 50% WNT3A-conditioned medium, 20% R-spondin-conditioned medium, 1× B27, 1× N-2, 10 mM nicotinamide (Sigma-Aldrich, N0636), 1.25 mM *N*-acetyl-L-cysteine (Sigma-Aldrich, A9165), 100 mg ml<sup>-1</sup> primocin (InvivoGen, ant-pm-2), 0.5 mM A83-01 (Tocris, 2939), 10 nM gastrin (Sigma, G9145), 4 nM R-spondin (R&D Systems, 4645-RS-100), 4 nM noggin (R&D Systems, 6057-NG-100), 5 nM fibroblast growth factor (R&D Systems, 345-FG-250), 5 ng ml<sup>-1</sup> epidermal growth factor (R&D Systems, 236-EG-200), 3 μM p38i SB202190 (Sigma-Aldrich, S7067) and 10 mM Rho-kinase inhibitor Y-27632 (Sigma-Aldrich, Y0503)). PDOs were serially passaged at confluence by mechanical disruption of cooled Matrigel domes (1 h, 4 °C) using Corning Cell Recovery Solution (Corning). Organoids were dissociated enzymatically with Tryple E (Gibco) at 37 °C for 5 min followed by brief (1–2 s) mechanical disruption using a 20-gauge needle. Dissociated organoids were pelleted by centrifugation (200g, 5 min) in culture medium (DMEM/F12 + 10% FBS + 1% penicillin–streptomycin) before resuspension in Matrigel for plating or expansion. After Matrigel polymerization (37 °C, 15 min), basal growth medium with Rho-Kinase inhibitor was added. For PDO viability assays, organoids were seeded at a concentration of 1 × 10<sup>4</sup> cells per well in a 96-well plate coated with Matrigel. The cells were incubated for 24 h before addition of TNF (10 ng ml<sup>-1</sup>) + IFNγ (10 ng ml<sup>-1</sup>), TBK1i (1 μM) or combination TNF/IFNγ + TBK1i in basal growth medium in 2% Matrigel in triplicate. Organoids were treated for 12 days in total with inhibitors/cytokines refreshed every 4 days. On day 12, viability assessment was performed using the 3D CellTiter-Glo (Promega) kit according to the manufacturer's protocol by adding 80 μl of CellTiter-Glo 3D Reagent to each well. The plate was incubated at room temperature for 30 min before recording the luminescence using the plate reader.

### BH3 profiling

B16 cells (*Tbk1* sgRNA 1 and 2 and control sgRNA 1 and 2) were isolated, centrifuged at 200g for 5 min and analysed using flow-cytometry-based BH3 profiling, as previously described<sup>61</sup>. In brief, cells were treated with BIM (peptide sequence, Ac-MRPEIWAQELRRIGDEFNA-NH<sub>2</sub>) or PUMA (peptide sequence, Ac-EQWAREIGAQLRRMADDLNA-NH<sub>2</sub>) BH3 peptides (Vivitide) for 60 min at 28 °C in MEB (10 mM HEPES (Sigma Aldrich) pH 7.5, 150 mM mannitol (Sigma Aldrich), 50 mM KCl (Sigma-Aldrich), 0.02 mM EGTA (Sigma-Aldrich), 0.02 mM EDTA (Sigma-Aldrich), 0.1% BSA (Jackson ImmunoResearch), 5 mM succinate (Sigma-Aldrich)) with 0.001% digitonin (Sigma-Aldrich). Alamethicin (Sigma-Aldrich) at 0.25 μM and DMSO at 1% were used as positive and negative controls, respectively. After peptide exposure, cells were fixed in 2% paraformaldehyde for 15 min, which was then neutralized by the addition of N2 buffer (1.7 M Tris base, 1.25 M glycine, pH 9.1). Cells were stained overnight with DAPI (1:1,000, Abcam) and anti-cytochrome-c-AlexaFluor647 (1:2,000, 6H2.B4, BioLegend) in a saponin-based buffer (final concentration, 0.1% saponin (Sigma-Aldrich), 1% BSA) and then analysed using flow cytometry. Cytochrome *c* release in response to treatment was measured on an Attune NxT flow cytometer (Thermo Fisher Scientific) from the DAPI<sup>+</sup> population. A greater cytochrome-*c*-negative

percentage indicates a greater response to peptide treatment. To evaluate the effect of TNF + IFNγ on apoptotic priming, BH3 profiling was performed as above at the indicated time points after treatment with TNF (160 ng ml<sup>-1</sup>) and IFNγ (40 ng ml<sup>-1</sup>).

### Annexin V/propidium iodide viability assay

Cells were plated at 10<sup>4</sup> cells per well in 100 μl culture medium on flat-bottom 96-well plates (Nest Scientific) and treated with TNF (160 ng ml<sup>-1</sup>) and IFNγ (40 ng ml<sup>-1</sup>) alone or in combination and co-treated with JAK1/2i (0.5 or 1 μM ruxolitinib) or TBK1i (0.25 or 1 μM). All combination treatments were performed with simultaneous administration. After 12, 18, 24 or 48 h under standard tissue culture conditions, the medium was collected and moved to a fresh 96-well V-bottom plate (Greiner Bio-One). Trypsin (25 μl, 0.0025%; Gibco) was added to each well on the original plate, allowed to incubate for 5 min and trypsinized cells were then added back to the medium on the V-bottom plate and stained with viability markers AxV and PI using the following protocol. A staining solution was prepared with 10× annexin binding buffer (0.1 M HEPES (pH 7.4), 1.4 M NaCl and 25 mM CaCl<sub>2</sub> solution, sterile filtered) and AxV/PI. AlexaFluor488-conjugated AxV (a gift from A. Letai) and PI (Abcam) was added to solution at a dilution of 1:500. The staining solution was then added to the cells in solution at 1:10 dilution and the cells were allowed to stain for 20 min on ice in the dark. AxV/PI positivity was then measured on the Attune NxT flow cytometer equipped with an autosampler (Thermo Fisher Scientific).

### Western blotting

Whole-cell lysates were prepared in RIPA Lysis Buffer (Millipore Sigma, 20-188). Protein concentration was measured using the BCA protein assay kit (Pierce). Samples clarified by centrifugation and boiled at 95 °C in 4× fluorescence-compatible sample buffer (Invitrogen). Protein lysates (30–50 mg) were loaded onto 4–12% Bolt Bis-Tris Plus gels (Life Technologies) in MES buffer (Life Technologies). Protein was transferred to a PVDF membrane using the iBLOT2 dry transferring system (Invitrogen). Membranes were blocked in Tris-buffered saline plus 0.1% Tween-20 (TBS-T) containing FL fluorescence blocking buffer (Thermo Fisher Scientific) for 1 h at room temperature followed by overnight incubation with primary antibodies at 4 °C. After washing, membranes were incubated with blocking buffer, and IRDye 800CW- or 680RD-conjugated secondary antibodies. Membranes were then visualized using the Odyssey CLx scanner (LI-COR), then analysed using ImageJ and Adobe Photoshop software. All data shown are representative of three independent experiments.

### RNA isolation and RT-qPCR

For BMDM RT-qPCR studies, cells were seeded in 12-well plates and cultured for 7 days. On day 8, TBK1i was added and, on day 9, LPS and IFNγ were added. After 2 h of LPS/IFNγ stimulation, total RNA was extracted from the cells using the RNeasy plus kit (Qiagen, 74034) according to the manufacturer's instructions. The mRNAs were quantified using the Power SYBR Green qPCR kit (Applied Biosystems, 4389986) with the company's protocol on the Thermo (Applied Biosystems) QStudio 6 FLX real-Time PCR System (105969). The following primers were used: *Tnf*, forward 5'-CCCTCACTCAGATCATCTTCT-3' and reverse 5'-GCTACGACGTGGGCTACAG-3'; *Il1a*, forward 5'-CGAA GACTACAGTTCTGCCATT-3'; and reverse 5'-GACGTTTTCAGAGGTTTCAGAG-3'; 18s, forward 5'-GCAATTATCCCCATGAACG-3' and reverse 5'-GGCCTCACTAAACCATCCAA-3'. Levels of mRNAs of interest were normalized to 18s using the formula 2<sup>C<sub>t</sub>(18s) - C<sub>t</sub>(mRNA X)</sup>. The resulting normalized ratio was presented in the figures. For B16 RT-qPCR studies, cells were seeded into 60 mm dishes (2 × 10<sup>6</sup> per dish) and cultured for 24 h at 37 °C. The cells were treated with TNF (160 ng ml<sup>-1</sup>) and IFNγ (40 ng ml<sup>-1</sup>) or PBS for 19 h. Total RNA was extracted from the cells using the RNeasy micro kit (Qiagen, 74004) according to the manufacturer's instructions. The mRNAs were quantified using the Blaze Taq one-step SYBR Green RT-qPCR

# Article

kit (GeneCopoeia, QP070) according to the manufacturer's protocol on the ROCHE Lightcycler-96 system. The following primers were used: *Mkl1*, forward 5'-TGAGGGAAGCTGCTGGATAGA-3' and reverse 5'-CCGAATGGTGTAGCTGTATAA-3'; *Ripk3*, forward 5'-GCACTCC TCAGATTCCACATAC-3' and reverse 5'-GTGTCTCCATCTCCCTGATTC-3'; *Actb*, forward 5'-GAGGTATCTGACCCCTGAAGTA-3' and reverse 5'-CACACGCAGCTCATTGTAGA-3'. Levels of mRNAs of interest were normalized to *Actb* using the formula  $2C_t(Actb) - C_t(mRNA X)$ . The resulting normalized ratio was presented in the figures.

## Antibodies

For western blotting, primary antibodies against TBK1 (ab40676, Abcam), IKK $\epsilon$  (3416T, Cell Signaling), p-RIPK S166/T169 (31122S, Cell Signaling), RIPK1 (3493S, Cell Signaling), cleaved caspase 8 (9429S, Cell Signaling), cleaved caspase 3 (9661T Cell Signaling), cleaved PARP (6544, Cell Signaling), c-FLIP (56343S, Cell Signaling), p-STAT1 Y701 (9167S, Cell Signaling), STAT1 (14994S, Cell Signaling), STING (13647S, Cell Signaling), p-IRF3 (29047S, Cell Signaling), IRF3 (4302S, Cell Signaling), p-JAK1 (74129T, Cell Signaling), JAK1 (3344T, Cell Signaling), p-JAK2 (8082T, Cell Signaling), JAK2 (3230T, Cell Signaling), p-p65 (3033T, Cell Signaling), p65 (8242T, Cell Signaling), p-MLKL S345 (37333, Cell Signaling) and MLKL (37705, Cell Signaling). Primary antibodies were used at 1:1,000 dilution in LI-COR Blocking Buffer. IRDye secondary antibodies against rabbit IgG, mouse IgG or goat IgG were purchased from LI-COR Biosciences (Invitrogen) and used at 1:10,000.  $\beta$ -Actin-680 (MA5-15739-D680, Invitrogen) was used as a loading control. Flow cytometry antibodies are listed above.

## Plasma collection and OLINK plasma proteomics assay

Patients with metastatic melanoma at Massachusetts General Hospital provided written informed consent for the collection of blood samples (DF/HCC IRB approved protocol, 11-181). Whole blood was collected in BD Vacutainer CPT tubes (BD362753) before treatment ( $n = 179$ ; 93 responders, 86 non-responders) and during treatment with ICB after 6 weeks ( $n = 173$ ; 93 responders, 80 non-responders) and after 6 months ( $n = 151$ ; 88 responders, 63 non-responders). Plasma (3 ml) was isolated after centrifuging CPT tubes containing whole blood for 25–30 min at room temperature and was subsequently stored at  $-80^\circ\text{C}$ . Olink Proximity Extension Assay (PEA) for high-multiplex analysis of proteins was performed as previously described<sup>62</sup>. In brief, oligonucleotide-labelled monoclonal or polyclonal antibodies (PEA probes) were used to bind to target proteins in a pairwise manner, facilitating hybridization when the oligonucleotides are in close proximity, followed by an extension step that generates a unique sequence used for digital identification of the analyte using next-generation sequencing. The full library (Olink Explore 1536) consists of 1,472 proteins and 48 control assays, divided into four 384-plex panels. Four overlapping assays of IL-6, IL-8 (CXCL8) and TNF were included for quality-control purposes. In the immune reaction, 2.8 ml of the sample was mixed with PEA probes and incubated overnight at  $4^\circ\text{C}$ . NPX is Olink's relative protein quantification unit on a  $\log_2$  scale and values are calculated from the number of matched counts on the NovaSeq run. Data generation of NPX consists of normalization to the extension control (known standard),  $\log_2$ -transformation and level adjustment using the plate control (plasma sample).

## Secreted cytokine profiling

Multiplexed analysis of secreted cytokines was performed using the MILLIPLEX MAP Human Cytokine/Chemokine Magnetic Bead Panel (HCYT MAG-60K-PX30). Conditioned medium samples (25  $\mu\text{l}$ ) from PDOTS were assayed neat. Concentration levels (pg  $\text{ml}^{-1}$ ) of each protein were derived from five-parameter curve-fitting models. Fold changes relative to the control samples were calculated and plotted as the  $\log_2$ -transformed fold change. Lower and upper limits of quantification (LLOQ/ULOQ) were imputed from standard curves for cytokines above or below detection.

## CRISPR sgRNA sequences

The following target sequences for CRISPR interference were designed using the sgRNA designer (<http://portals.broadinstitute.org/gpp/public/analysis-tools/sgRNA-design>): Control sgRNA 1 ATTGTTCGACCGTC-TACGGG; Control sgRNA 2 ACGTGTAAAGCGAAGCCCTT; *Tbk1* sgRNA 1 CGGGAACAACCAATACCGT; *Tbk1* sgRNA 2 GACCGTCCACAAGAA-GACGG; *Tmem173* (*Sting1*) sgRNA 1 GAAGGCCAAACATCCACTG; and *Irf3* sgRNA 1 GCATGGAAACCCCGAAACCG.

## Sanger sequencing

B16 clones were collected and DNA was extracted using 50  $\mu\text{l}$  QuickExtract DNA Extraction Solution (Lucigen). PCR was performed on 1  $\mu\text{l}$  of the extracted DNA solution using Herculase II Fusion DNA Polymerase (Agilent Technologies) according to the manufacturer's protocol for targets of <1 kb. PCR primers were designed to target the region of the *Tbk1* gene flanking the expected CRISPR-Cas9 cut site. The *Tbk1* sgRNA 1 cut site forward primer was CCTTCTGACGTCCCTCACAG. The *Tbk1* sgRNA 1 cut site reverse primer was ACTGGTGAAGTTATGATGGA.

PCR products were purified using the QIAquick PCR Purification Kit (Qiagen). PCR bands were visualized using the E-Gel Power Snap Electrophoresis System (Invitrogen). Sanger sequencing was performed at the MGH CCIB DNA Core using the ABI 3730XL DNA Analyzer (Thermo Fisher Scientific). Sanger sequencing results were analysed using the Synthego Inference of CRISPR Edits (ICE)<sup>63</sup> and Tracking of Indels by DEcomposition (TIDE)<sup>64</sup> software tools to determine insertions and deletions at the CRISPR cut site. Next-generation sequencing was subsequently performed to confirm the Sanger sequencing results.

## Source data

scRNA-seq data for CD45<sup>+</sup> cells (SMART-Seq2) from patients with melanoma treated with ICB were previously described<sup>23</sup> (Gene Expression Omnibus (GEO): GSE120575). In each sample, the fraction of cells with a non-zero expression of either *IFNG*, *TNF* or both was calculated. Wilcoxon rank-sum tests were then used to determine the significance level of the difference between responding and non-responding patients. The Broad Single Cell Viewer ([https://singlecell.broadinstitute.org/single\\_cell](https://singlecell.broadinstitute.org/single_cell)) was used for evaluation of *TBK1* and *IKBKE* expression in CD45<sup>+</sup> immune cells from human patients with melanoma. Bulk RNA-seq data from B16 cells treated with TNF, IFN $\gamma$  or TNF/IFN $\gamma$  compared with untreated controls were previously described (GEO: GSE99299).

## Statistical methods, data analysis and software

The statistical tests used with the number of replicates and independent experiments are listed in the text and figure legends. All graphs with error bars report mean  $\pm$  s.e.m. values except where otherwise indicated. *t*-tests were two-tailed in all cases. GraphPad/Prism (v.9.0) was used for basic statistical analysis and plotting (<http://www.graphpad.com>). The R language and programming environment (<https://www.r-project.org>) was used for the remainder of the statistical analysis. Multiple-hypothesis testing correction was applied where multiple hypotheses were tested and is indicated by the use of FDR. The data analysis software used included GraphPad/Prism (v9.0), Microsoft Excel (v.15), FlowJo (v.10), NIS Elements (v.5.11), Cell Ranger (v.3.0), Scanpy (v.1.4.5post3), scran (v.1.14.6) and MetaXpress (v.6.5.3.427). Schematics were generated using BioRender.

## Reporting summary

Further information on research design is available in the Nature Portfolio Reporting Summary linked to this article.

## Data availability

The datasets generated and analysed in this study are included in the Article and its Supplementary Information. In vivo scRNA-seq data

have been deposited at the GEO under the accession codes GSE217160 (in vivo TBK1 study) and GSE217274 (in vivo TBK1 CRISPR–Cas9 study) and are available on request. Descriptions of the analyses are provided in the Methods and Reporting summary.

52. Deng, R. et al. Preclinical pharmacokinetics, pharmacodynamics, tissue distribution, and tumor penetration of anti-PD-L1 monoclonal antibody, an immune checkpoint inhibitor. *MAbs* **8**, 593–603 (2016).
53. Wolf, F. A., Angerer, P. & Theis, F. J. SCANPY: large-scale single-cell gene expression data analysis. *Genome Biol.* **19**, 15 (2018).
54. Korsunsky, I. et al. Fast, sensitive and accurate integration of single-cell data with Harmony. *Nat. Methods* **16**, 1289–1296 (2019).
55. Ntranos, V., Yi, L., Melsted, P. & Pachter, L. A discriminative learning approach to differential expression analysis for single-cell RNA-seq. *Nat. Methods* **16**, 163–166 (2019).
56. Subramanian, A. et al. Gene set enrichment analysis: a knowledge-based approach for interpreting genome-wide expression profiles. *Proc. Natl Acad. Sci. USA* **102**, 15545–15550 (2005).
57. Doench, J. G. et al. Optimized sgRNA design to maximize activity and minimize off-target effects of CRISPR-Cas9. *Nat. Biotechnol.* **34**, 184–191 (2016).
58. Doench, J. G. et al. Rational design of highly active sgRNAs for CRISPR-Cas9-mediated gene inactivation. *Nat. Biotechnol.* **32**, 1262–1267 (2014).
59. Lu, H. et al. PAK signalling drives acquired drug resistance to MAPK inhibitors in BRAF-mutant melanomas. *Nature* **550**, 133–136 (2017).
60. van de Wetering, M. et al. Prospective derivation of a living organoid biobank of colorectal cancer patients. *Cell* **161**, 933–945 (2015).
61. Fraser, C., Ryan, J. & Sarosiek, K. BH3 profiling: a functional assay to measure apoptotic priming and dependencies. *Methods Mol. Biol.* **1877**, 61–76 (2019).
62. Filbin, M. R. et al. Longitudinal proteomic analysis of severe COVID-19 reveals survival-associated signatures, tissue-specific cell death, and cell-cell interactions. *Cell Rep. Med.* **2**, 100287 (2021).
63. Conant, D. et al. Inference of CRISPR edits from Sanger trace data. *CRISPR J.* **5**, 123–130 (2022).
64. Brinkman, E. K., Chen, T., Amendola, M. & van Steensel, B. Easy quantitative assessment of genome editing by sequence trace decomposition. *Nucleic Acids Res.* **42**, e168 (2014).

**Acknowledgements** This work was supported by NIH K08CA226391 (to R.W.J.), P01CA24023 (to S.I.P.), K99CA259511 (to K.P.), T32CA207021 (to J.H.C.), 5R01AR072304 (to D.E.F.), 5P01CA163222 (to D.E.F.), 5R01AR043369 (to D.E.F.) and 5R01CA222871 (to D.E.F.). Additional support was provided by the Melanoma Research Alliance Young Investigator Award (<https://doi.org/10.48050/pc.gr.86371>, to R.W.J.), a Karin Grunebaum Cancer Research Foundation Faculty Research Fellowship (to R.W.J.), Termeer Early Career Fellowship in Systems Pharmacology (to R.W.J.) and a gift from S. B. and J. W. Belkin. K.P. acknowledges support from the German Research Foundation (DFG), Stand Up to Cancer Peggy Prescott Early

Career Scientist Award PA-6146, Stand Up to Cancer Phillip A. Sharp Award SU2C-AACR-PS-32; D.J. acknowledges the Susan Eid Tumor Heterogeneity Initiative; and D.E.F. acknowledges grant support from the Dr Miriam and Sheldon G. Adelson Medical Research Foundation. The funding bodies had no role in the design of the study, and the collection, analysis and interpretation of the data, or in writing the manuscript. We thank all members of the Manguso and Jenkins laboratories at MGH, HMS and the Broad Institute. Graphics in Figs. 2a and 5i were created using BioRender.

**Author contributions** Conception and experimental design: Y.S., O.-y.R., S.A., C.E.M., P.T., K.B.Y., A.I.-V., R.T.M. and R.W.J. Methodology and data acquisition: Y.S., O.-y.R., S.A., E.A.K., C.H.W., A.J., C.E.M., E.J.R., A.F., X.M., J.G., P.T., A.M.C., M.Q.R., P.S., J.T., A.M., H.X., T.S., S.L., W.A.M., R.S.-B., J.K.E.S., X.Q., G.Z., M.Y.S., J.W.K., S.J.K., D.T.F., D.J., S.I.P., D.M.M., S.S., E.I., A.R.A., C.P.P., D.R.S. and G.M.B. Analysis and interpretation of data: Y.S., O.-y.R., S.A., C.E.M., P.T., T.G.R.D., S.K., P.P.D., J.T., A.M., A.M.S., K.Y., M.S.-F., T.L., J.W.K., K.A.S., A.G.-H., J.H.C., K.P., D.A.B., D.E.F., R.B.C., N.H., P.K.S., K.T.F., G.M.B., R.T.M. and R.W.J. Manuscript writing and revision: Y.S., O.-y.R., S.A., C.E.M., H.X., D.J., D.A.B., R.T.M. and R.W.J.

**Competing interests** R.W.J. is a member of the advisory board for and has a financial interest in Xspera Biosciences, a company focused on using ex vivo profiling technology to deliver functional, precision immune-oncology solutions for patients, providers and drug development companies. A.M. is a consultant for Third Rock Ventures, Asher Biotherapeutics and Abata Therapeutics; and holds equity in Asher Biotherapeutics and Abata Therapeutics. S.I.P. has received consultancy payments from Abbvie, AstraZeneca/MedImmune, Cue Biopharma, Fusion Pharmaceuticals, MSD/Merck, Newlink Genetics, Oncolys Biopharma, Replimmune, Scopus Biopharma and Sensei Biopharma; she has received grants/research support from Abbvie, AstraZeneca/MedImmune, Cue Biopharma, Merck and Tesaro. S.J.K. has served a consultant/advisory role for Eli Lilly, Merck, BMS, Astellas, Daiichi-Sankyo, Pieris and Natera; and owns stock in Turning Point Therapeutics. D.J. received consulting fees from Novartis, Genentech, Syros, Eisai, Vibliome, Mapkure and Relay Therapeutics; conducted contracted research with Novartis, Genentech, Syros, Pfizer, Eisai, Takeda, Pfizer, Ribon Therapeutics, Infinity, InventisBio and Arvinas; and has ownership interest in Relay Therapeutics and PIC Therapeutics. D.M.M. has received honoraria for participating on advisory boards for Checkpoint Therapeutics, EMD Serono, Castle Biosciences, Pfizer, Merck, Regeneron and Sanofi Genzyme; and owns stock in Checkpoint Therapeutics. D.E.F. has a financial interest in Soltego, a company developing salt-inducible kinase inhibitors for topical skin-darkening treatments that might be used for a broad set of human applications. R.T.M. consults for Bristol Myers Squibb. M.S.-F. receives research funding from Bristol-Meyers Squibb.

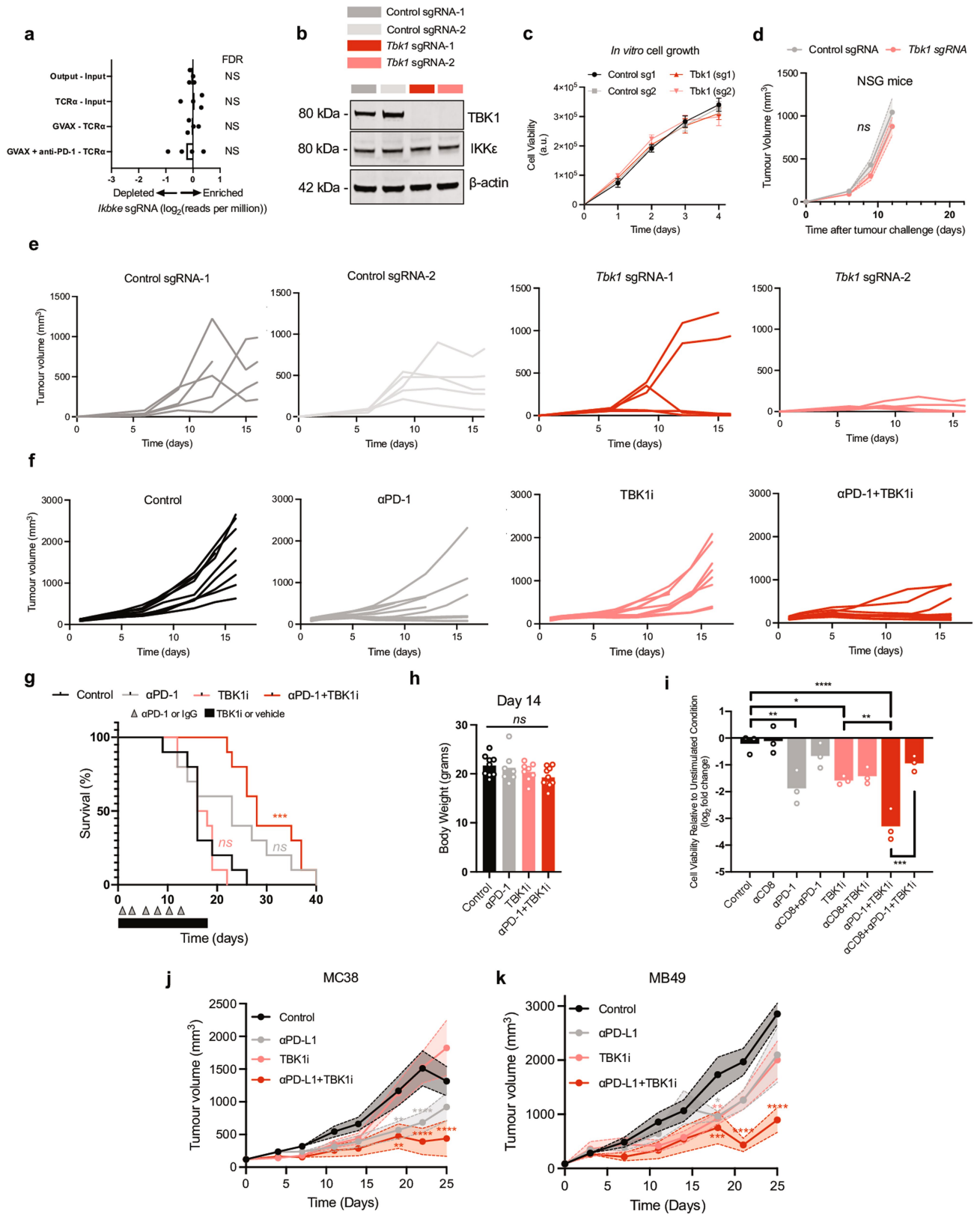
#### Additional information

**Supplementary information** The online version contains supplementary material available at <https://doi.org/10.1038/s41586-023-05704-6>.

**Correspondence and requests for materials** should be addressed to Russell W. Jenkins.

**Peer review information** Nature thanks Robert Bradley, Toshiro Sato and the other, anonymous, reviewer(s) for their contribution to the peer review of this work. Peer reviewer reports are available.

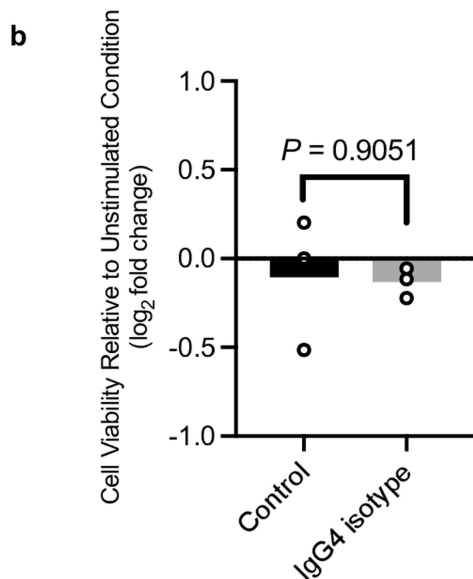
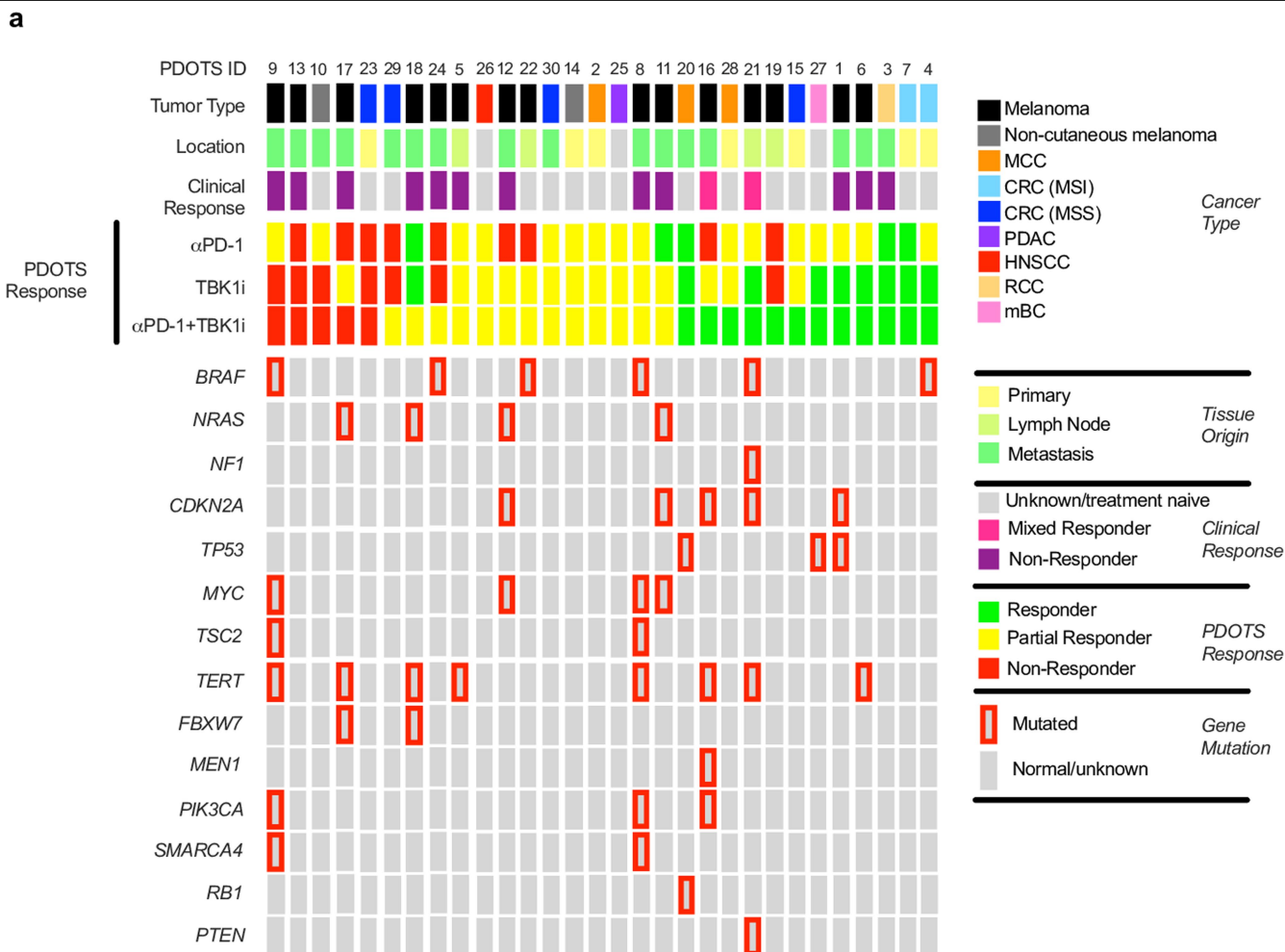
**Reprints and permissions information** is available at <http://www.nature.com/reprints>.



Extended Data Fig. 1 | See next page for caption.

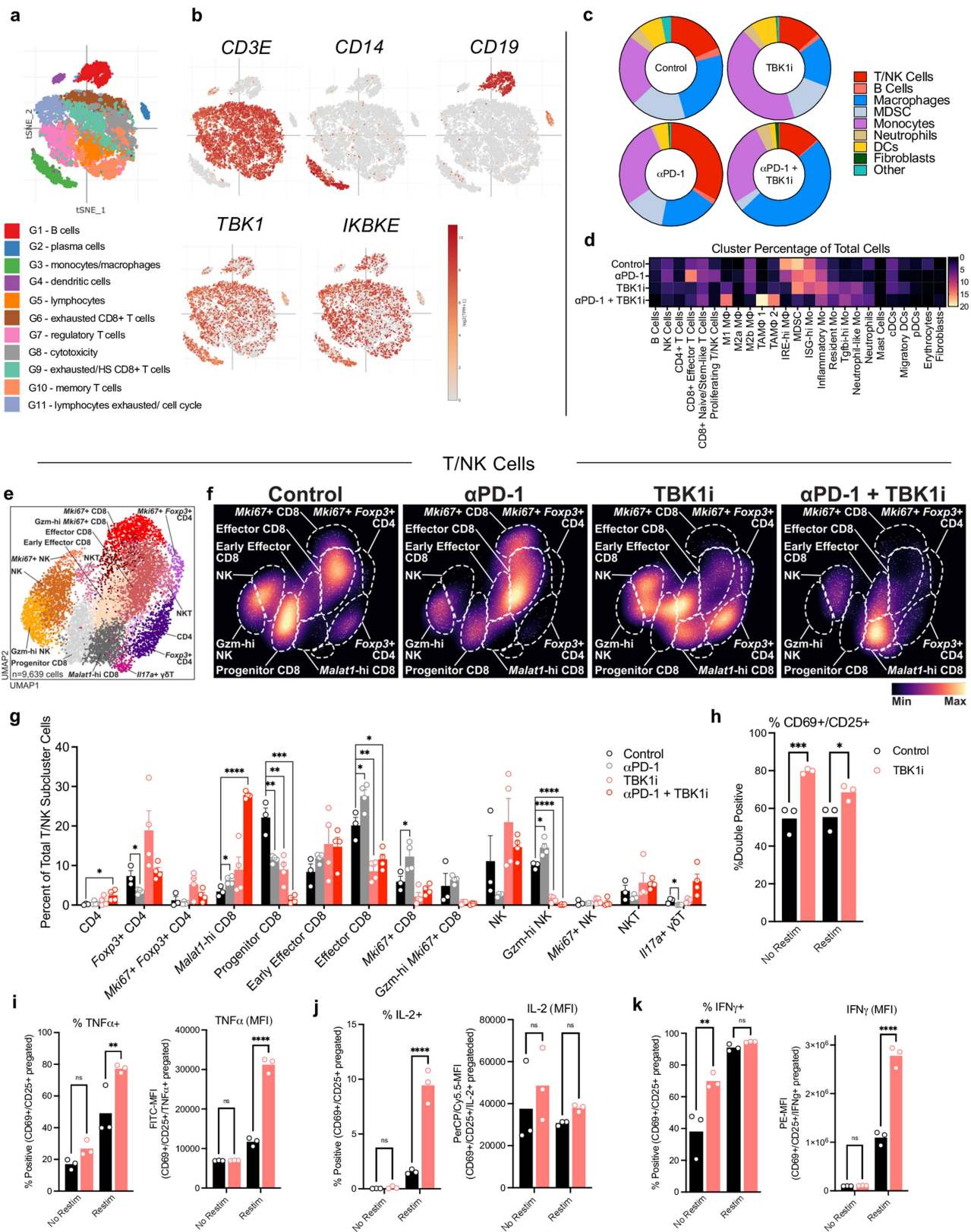
**Extended Data Fig. 1 | Supporting evidence that loss of TBK1 sensitizes tumours to cancer immunotherapy.** **a**, Relative depletion/enrichment of *Ikbke* sgRNAs from a pool of sgRNAs targeting 2,368 genes expressed by Cas9-expressing B16 melanoma cells ( $n = 4$  independent guides targeting each gene; false discovery rate (FDR) was calculated using the STARS algorithm v1.3, as previously described<sup>6,7</sup>). **b**, TBK1 and  $\beta$ -actin protein levels in control and *Tbk1*-null B16 cells. Results are representative of three independent experiments. **c**, Proliferation of *Tbk1*-null and control B16 tumour cells following at 1-4 days of *in vitro* culture ( $n = 9$  per condition from three independent experiments). **d**, Tumour volume of control (grey), *Tbk1*-null (light red) B16 tumours in NSG mice ( $n = 5$  mice per group). Mean tumour volumes (solid circles) are shown  $\pm$  s.e.m. (shaded region). 2-way ANOVA with Sidak's multiple comparisons test. **e**, Spider plots for tumour volume analysis for control sgRNA-1 (black), sgRNA-2 (grey), *Tbk1* sgRNA-1 (pink), and *Tbk1* sgRNA-2 (red) B16 tumours in anti-PD-1-treated wild-type C57BL/6 mice (see Fig. 1c). **f-g**, Spider plots for tumour volume analysis (f) and survival (g) for control (black), anti-PD-1 (grey), TBK1i (pink), and

anti-PD-1+TBK1i (red) B16 tumours in C57BL/6 mice (see Fig. 1d). For survival analysis (g), pairwise testing was performed using the log-rank (Mantel-Cox) test for survival (g);  $n = 10$  mice per treatment group,  $***P < 0.001$ ; *ns*, not significant, compared to control group. **h**, body weight of mice bearing B16-ova tumours on Day 14 of indicated treatment. Means (bars) and individual values (open circles) are shown ( $n = 10$  mice per group, 1-way ANOVA with Tukey's multiple comparisons test; *ns*, not significant). **i**, Viability assessment of CT26 MDOTs with indicated treatments. Means (bars) and individual values (open circles) are shown ( $n = 3$ , biological replicates, one-way ANOVA with Tukey's multiple comparisons test;  $*P < 0.05$ ;  $**P < 0.01$ ;  $***P < 0.001$ ;  $****P < 0.0001$ ). **j-k**, Tumour volume analyses of mice bearing MC38 (j) and MB49 (k) tumours treated with TBK1i, anti-PD-L1, or combination compared to control (IgG + vehicle);  $n = 10$  mice per treatment group. Mean tumour volumes (solid circles) are shown  $\pm$  s.e.m. (shaded region). 2-way ANOVA with Tukey's multiple comparisons test  $***P < 0.001$ ; compared to control group.



**Extended Data Fig. 2 | Supporting data that TBK1 inhibition enhances sensitivity to PD-1 blockade using PDOTS. a**, Tumour type, tissue source (location), clinical response data, PDOTS response data, and associated tumour mutation profile for specimens used for PDOTS profiling (samples ordered by *ex vivo* PDOTS response to combined anti-PD-1+TBK1i). PDOTS response parameters defined as follows: responder (reduction >30% compared

to control), partial responder (<30% reduction and <20% growth compared to control), and non-responder (>20% growth compared to control). Red border around grey rectangle indicates presence of alteration in indicated gene. **b**, effect of IgG4 control monoclonal Ab on viability of PDOTS from a patient with melanoma. Means (bars) and individual values (open circles) are shown ( $n = 3$ , biological replicates, 2-sided unpaired *t*-test).

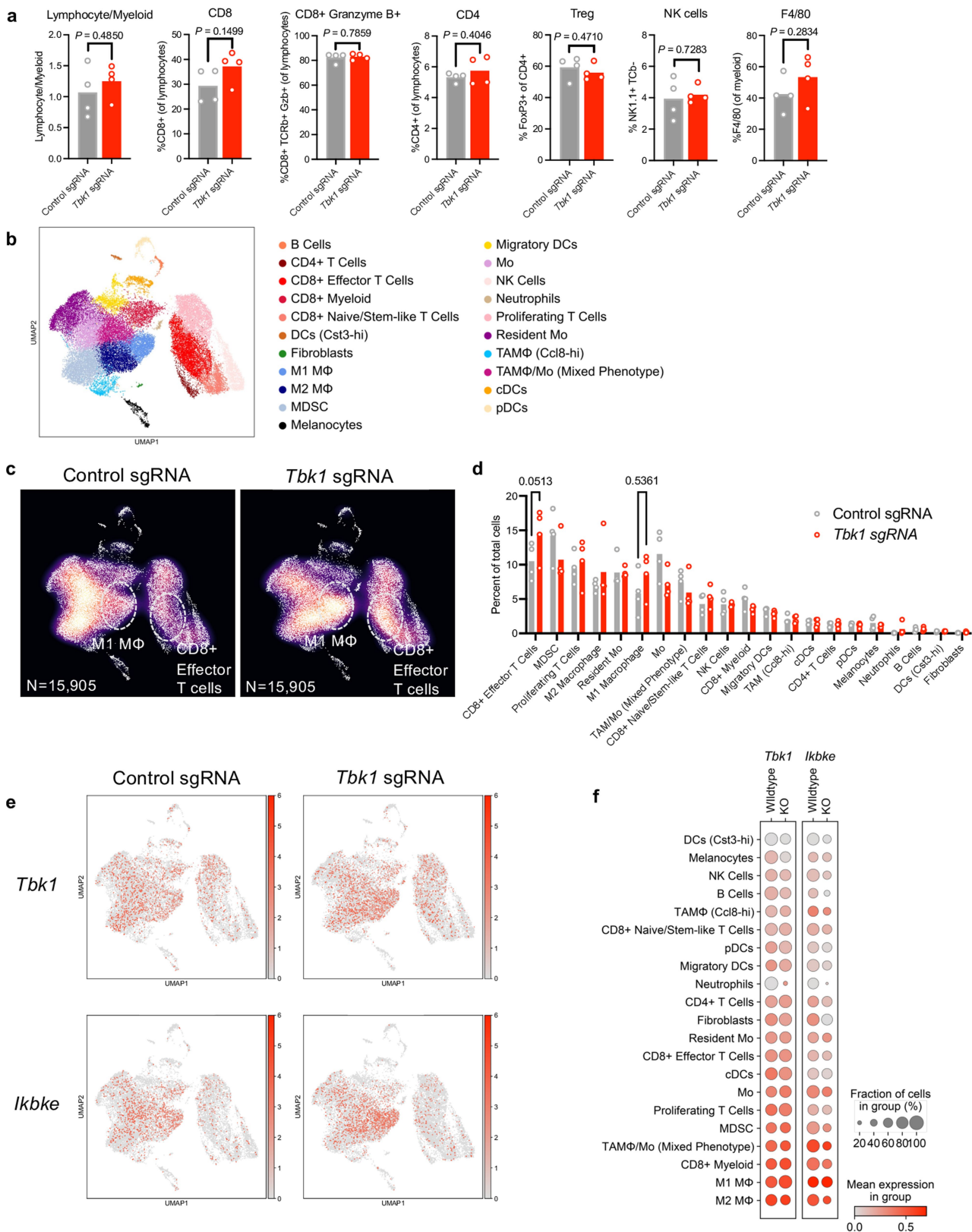


Extended Data Fig. 3 | See next page for caption.

# Article

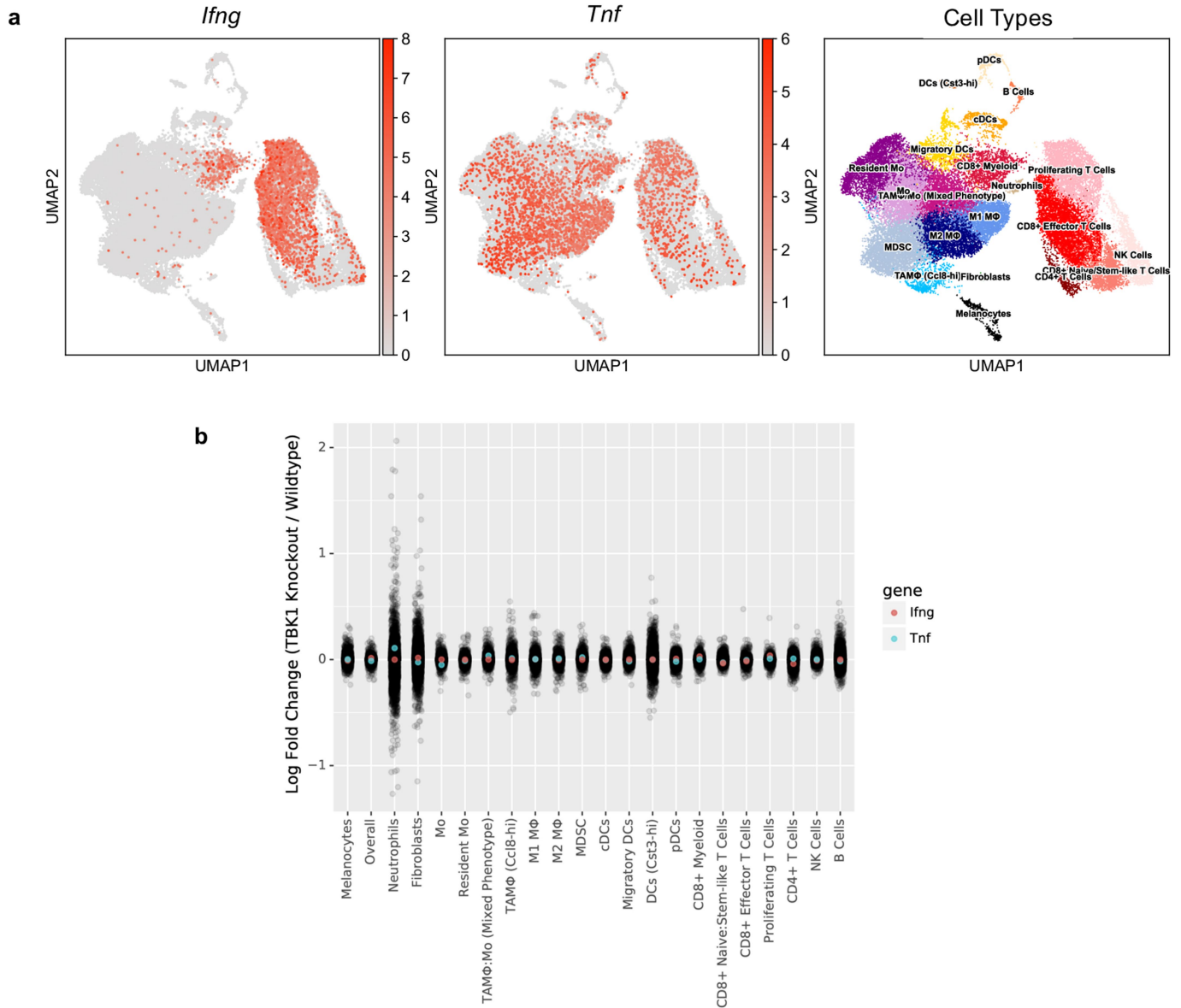
**Extended Data Fig. 3 | Effect of TBK1 inhibition on the tumour immune microenvironment.** **a–b**, tSNE plot of 11 clusters of CD45+ cells (a) from patients with metastatic melanoma responsive (R) or non-responsive (NR) to immune checkpoint blockade (ref. Sade-Feldman et al. 2018), and t-SNE plots of RNA-sequenced single cells with colouring of *CD3E* (T cells), *CD14* (myeloid cells), and *CD19* (B cells) *TBK1* and *IKBKE* expression (b). **c–d**, broad cluster proportions (c) and percent cells per cluster across indicated treatment groups (d). **e–f**, UMAP (e) and density (f) plots of reclustered lymphoid (T/NK) cells. **g**, cluster proportions of lymphoid (T/NK) cells. Means (bars) and individual values (circles) are shown +/- s.e.m (error bars). Multiple unpaired *t*-test, \**P* < 0.05; \*\**P* < 0.01; \*\*\**P* < 0.001;

\*\*\*\* *P* < 0.0001; *ns*, not significant. **h**, percentage of activated (CD69+CD25+) mouse CD8+ splenocytes pre-treated with TBK1i (1 μM) or DMSO (0.1%) with/without restimulation; n = 3 biologically independent samples, 2-way ANOVA, Sidak's multiple comparisons test; \**P* < 0.05; \*\*\**P* < 0.001. **i–k**, intracellular cytokine staining for TNF (i), IL-2 (j), and IFNγ (k) of mouse CD3+CD8+ splenocytes pre-treated with TBK1i (1 μM) or DMSO (0.1%) with/without restimulation with data shown as % CD69+CD25+ cells and MFI; n = 3 biologically independent samples, 2-way ANOVA, Sidak's multiple comparisons test; \*\**P* < 0.01; \*\*\*\* *P* < 0.0001; *ns*, not significant.

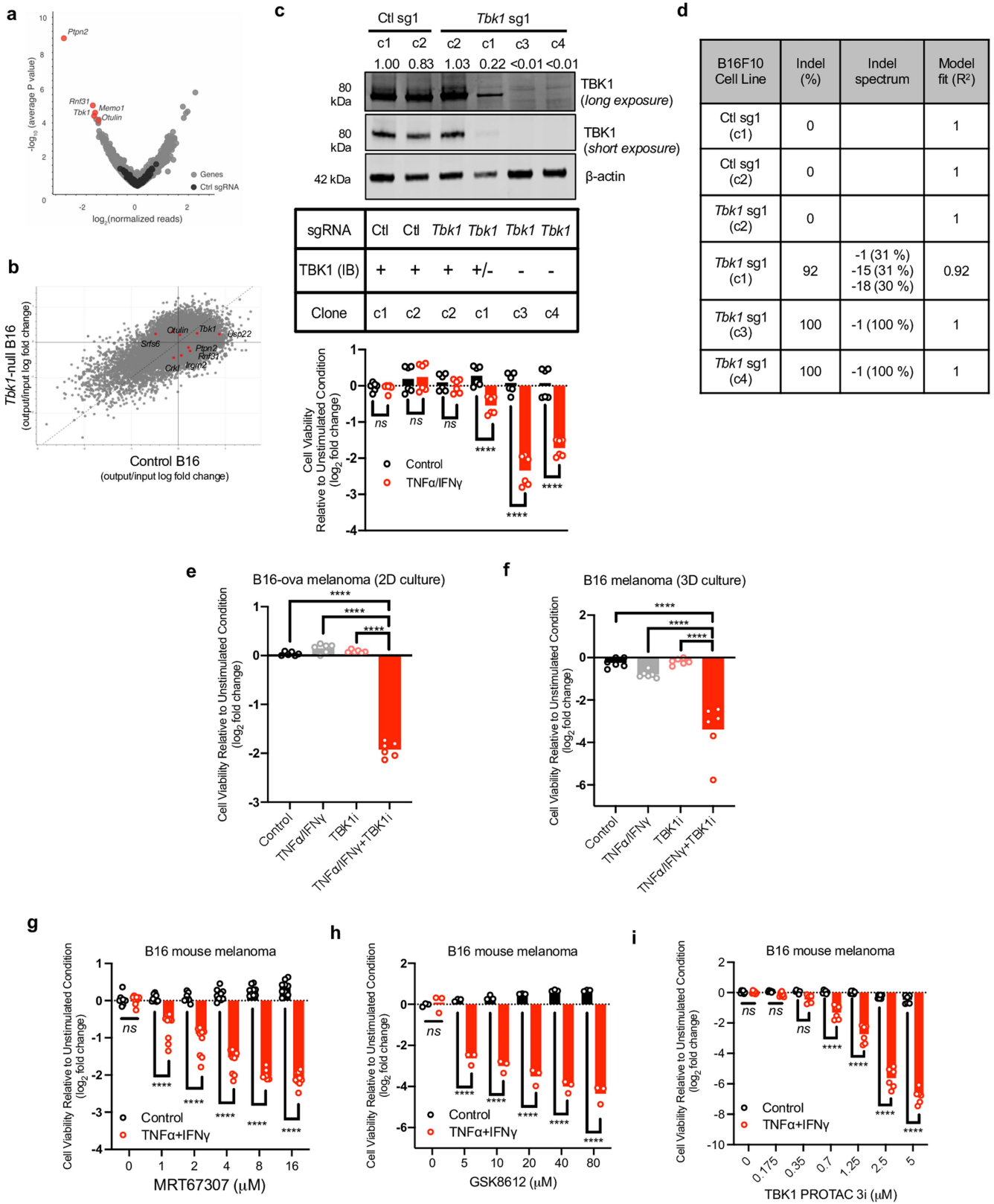


**Extended Data Fig. 4 | Effect of *Tbk1* deletion on the tumour immune microenvironment.** **a**, Flow cytometry of immune populations from control and *Tbk1*-null B16 tumours treated with anti-PD-1 ( $n = 4$  per group). Means (bars) and individual values (open circles) are shown ( $n = 4$  biologically independent samples, 2-sided unpaired  $t$ -test). **b-c**, UMAP (b) and density (c) plots of 31,810 RNA-sequenced single cells from control and *Tbk1*-null B16 tumours following anti-PD-1 treatment (DC, dendritic cells; Tregs, regulatory T cells; MDSC, myeloid-derived suppressor cell; NK, natural killer cells; M1, M1

macrophages; M2, M2 macrophages). **d**, percent of cells in each lineage-defined cluster. Means (bars) and individual values (open circles) are shown ( $n = 4$  biologically independent samples, 2-way ANOVA, Sidak's multiple comparisons test;  $P$  values shown for M1 macrophages and CD8 T cells that did not reach statistical significance). **e**, UMAP plot of RNA-sequenced single cells with colouring of *Tbk1* and *Ikbke* expression with cell types referenced (b). **f**, bubble plot indicating *Tbk1* and *Ikbke* expression across UMAP-defined cell clusters.



**Extended Data Fig. 5 | TNF and IFN $\gamma$  expression in B16 melanoma tumours. a**, UMAP plot of RNA-sequenced single cells with colouring of *Ifng* and *Tnf* expression with cell types referenced (right). **b**, log-fold change of *Ifng* (light red) and *Tnf* (light blue) expression across lineage-defined cell clusters (*Tbk1*-null/control).

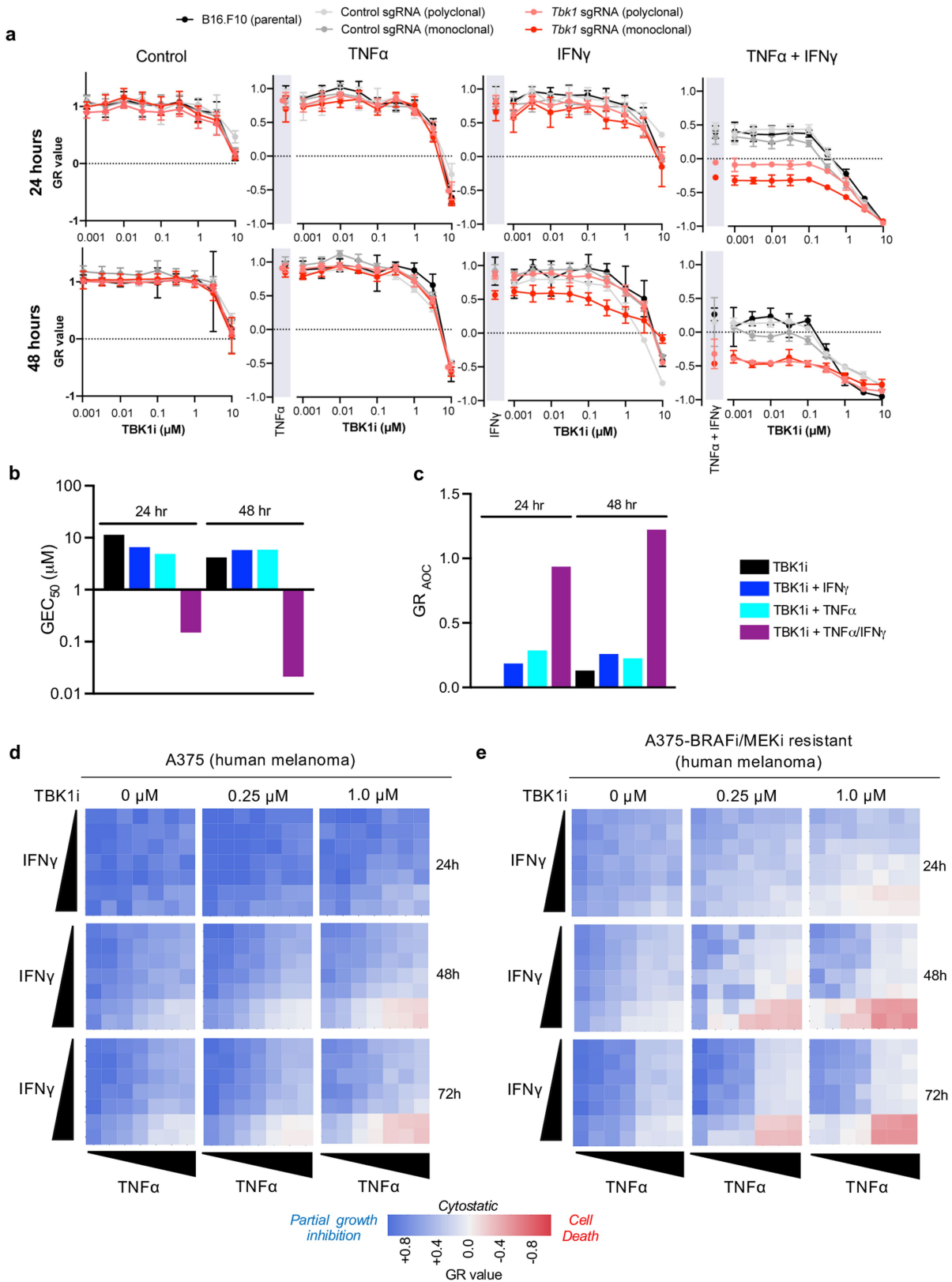


Extended Data Fig. 6 | See next page for caption.

# Article

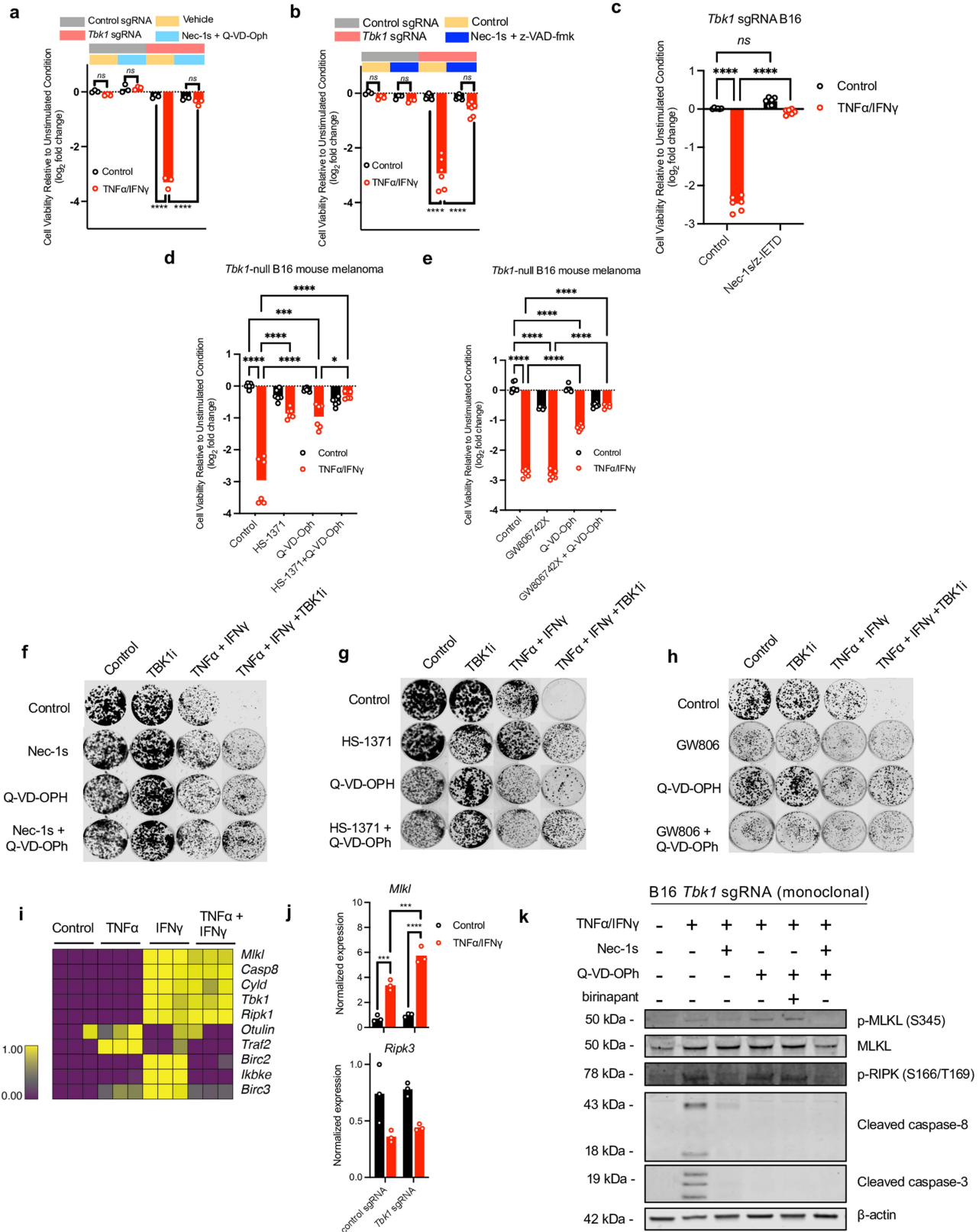
**Extended Data Fig. 6 | Supporting data that loss/inhibition of TBK1 sensitizes tumour cells to TNF/IFN $\gamma$ .** **a**, volcano plot depicting relative sgRNAs gene depletion/enrichment. Top 5 depleted sgRNAs indicated. **b**, scatter plot of gene essentiality from *in vitro* CRISPR screen (control and *Tbk1*-null B16 cells). **c**, TBK1 expression and cell viability (control vs. TNF/IFN $\gamma$ ) for single cell clones derived from polyclonal control and *Tbk1*-null B16 cells. Western blot is representative of three independent experiments. Means (bars) and individual values (open circles) are shown ( $n = 6$  across two independent experiments, 2-way ANOVA, Sidak's multiple comparisons test; \*\*\*\*  $P < 0.0001$ ; *ns*, not significant). **d**, TBK1 indel spectrum from control sgRNA and *Tbk1* sgRNA B16 single cell clones. **e**, Viability assessment (Cell Titer Glo) of B16-ova cells in standard 2D culture after 24 h treatment with TNF (160 ng ml $^{-1}$ ) + IFN $\gamma$  (40 ng ml $^{-1}$ ) compared to unstimulated cells ( $n = 6$ , 2 independent experiments, 1-way ANOVA, Holm-Sidak's multiple comparisons test). **f**, Viability assessment (Hoechst/propidium iodide) of B16 tumour spheroids

(lacking immune cells) in 3D microfluidic culture after 96 h treatment with TNF (10 ng ml $^{-1}$ ) + IFN $\gamma$  (10 ng ml $^{-1}$ ) compared to unstimulated cells ( $n = 6$ , 2 independent experiments, 1-way ANOVA, Holm-Sidak's multiple comparisons test). **g**, Cell viability assessment of B16 cells after 24 h treatment with TNF (200 ng ml $^{-1}$ ) + IFN $\gamma$  (40 ng ml $^{-1}$ ) compared to unstimulated cells treated with increasing concentrations of MRT67307 ( $n = 9$ , 3 independent experiments 2-way ANOVA, Sidak's multiple comparisons test). **h**, Cell viability assessment of B16 cells in standard 2D culture after 24 h treatment with TNF (200 ng ml $^{-1}$ ) + IFN $\gamma$  (40 ng ml $^{-1}$ ) compared to unstimulated cells treated with increasing concentrations of GSK8612 ( $n = 3$ , 1 independent experiment, 2-way ANOVA, Sidak's multiple comparisons test). **i**, Cell viability assessment of B16 cells in standard 2D culture after 24 h treatment with TNF (200 ng ml $^{-1}$ ) + IFN $\gamma$  (40 ng ml $^{-1}$ ) with increasing concentrations of TBK1 PROTAC 3i ( $n = 6$ , 2 independent experiments 2-way ANOVA, Sidak's multiple comparisons test). \*\*\*\*  $P < 0.0001$ ; *ns*, not significant.



**Extended Data Fig. 7 | Supporting data that TBK1 inhibition lowers the cytotoxicity threshold to TNF/IFN $\gamma$ .** **a**, GR values for 9-point inhibitor titration of TBK1i in parental, control sgRNA (polyclonal and monoclonal), and *Tbk1* sgRNA (polyclonal and monoclonal) B16 cells (2 independent experiments; representative data from single experiment with 6 technical replicates per condition). Means (solid circles) are shown  $\pm$  s.e.m (error bars). **b-c**, evaluation

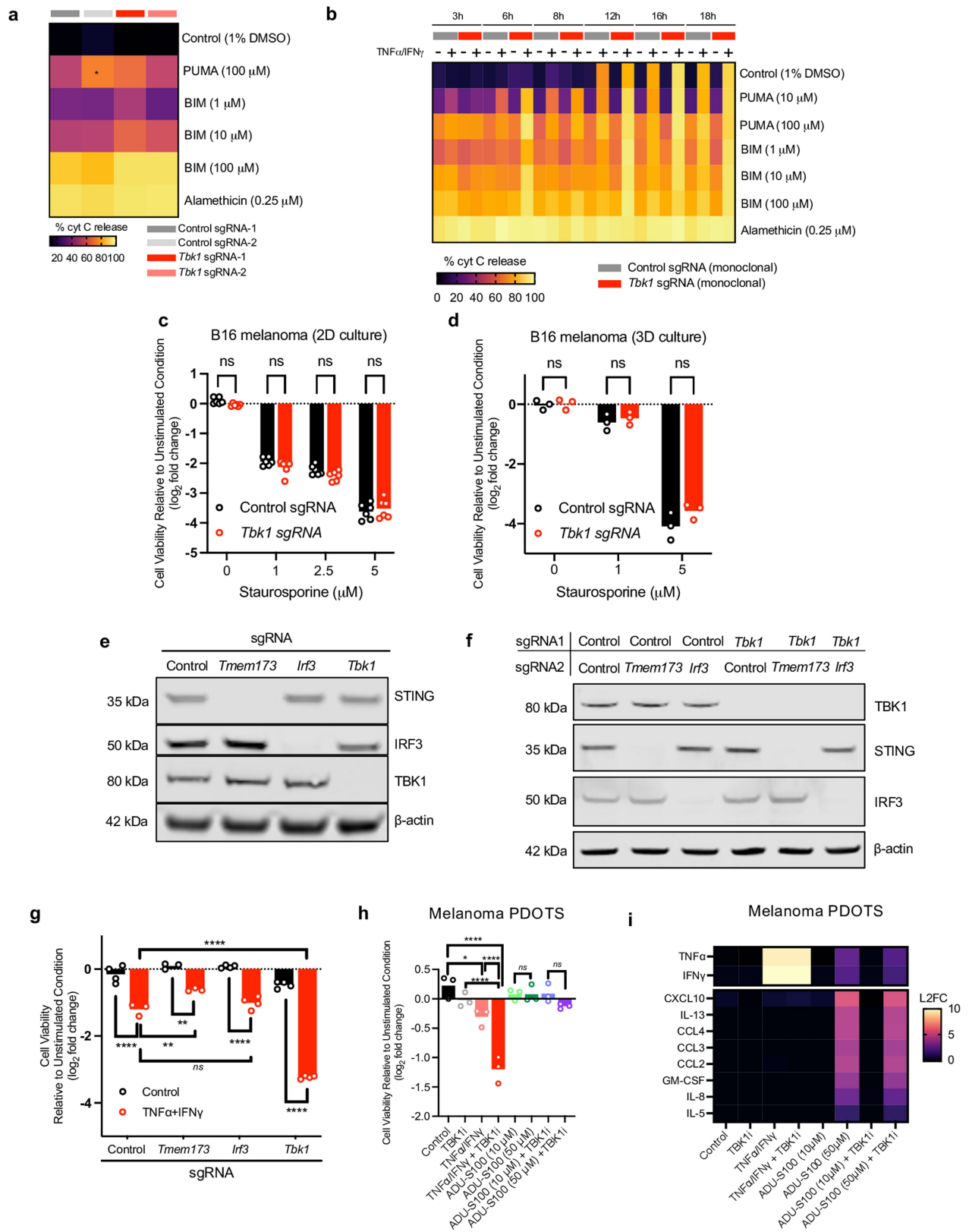
of TBK1i potency (b; half-maximal effect,  $GEC_{50}$ ) and overall efficacy (c; area over the GR curve,  $GR_{AOC}$ ). **d-e**, Heatmap of GR values for parental (d) and BRAF/MEK inhibitor resistant (e) A375 human melanoma cells treated with increasing concentrations of TNF and IFN $\gamma$  for 24, 24, and 72 h with 0, 0.25, and 1.0  $\mu$ M TBK1i (n = 3).



Extended Data Fig. 8 | See next page for caption.

**Extended Data Fig. 8 | Supporting data that *Tbkl*-null cells undergo RIPK and caspase-dependent cell death.** **a–b**, Cell viability assessment (Cell Titer Glo) in control and *Tbkl*-null B16 cells pre-treated with RIPK1 inhibitor (Nec-1s, 10  $\mu$ M) and the pan-caspase inhibitor Q-VD-OPh (10  $\mu$ M) +/- TNF/IFN $\gamma$  (n=3, 1 independent experiment: 2-way ANOVA, Dunnett's multiple comparisons test). **b**, cell viability assessment (Cell Titer Glo) in control and *Tbkl*-null B16 cells pre-treated with RIPK1 inhibitor (Nec-1s, 10  $\mu$ M) and the pan-caspase inhibitor z-VAD-fmk (20  $\mu$ M) +/- TNF/IFN $\gamma$  (n = 3-6, 1-2 independent experiments: 2-way ANOVA, Dunnett's multiple comparisons test). **c**, cell viability assessment in *Tbkl*-null B16 cells pre-treated with RIPK1 inhibitor (Nec-1s, 10  $\mu$ M) and the caspase 8 inhibitor z-IETD-fmk (2.5  $\mu$ M) +/- TNF/IFN $\gamma$  (n = 6, 2 independent experiments; 2-way ANOVA, Dunnett's multiple comparisons test). **d**, cell viability assessment in *Tbkl*-null B16 cells pre-treated with RIPK3 inhibitor (HS-1371, 2  $\mu$ M) and the pan-caspase inhibitor Q-VD-OPh (20  $\mu$ M) +/- TNF/IFN $\gamma$  (n = 6, 2 independent experiments: 2-way ANOVA, Dunnett's multiple comparisons test). **e**, cell viability assessment in *Tbkl*-null B16 cells pre-treated with MLKL inhibitor (GW806742X, 5  $\mu$ M) and the pan-caspase inhibitor Q-VD-

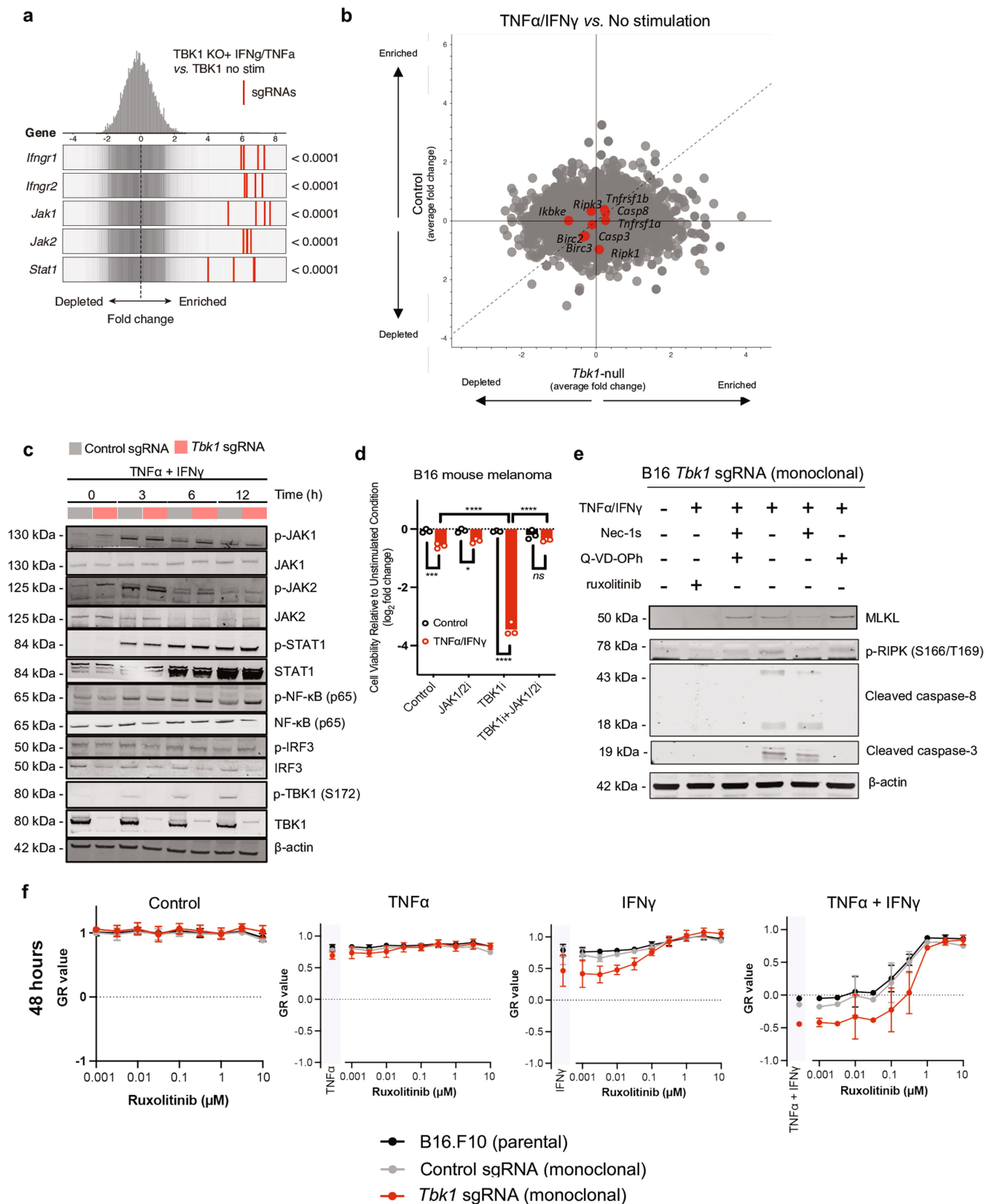
OPh (20  $\mu$ M) +/- TNF/IFN $\gamma$  (n = 6, 2 independent experiments: 2-way ANOVA, Dunnett's multiple comparisons test). **f–h**, Clonogenic assay of B16 cells treated with TNF (10 ng ml<sup>-1</sup>), IFN $\gamma$  (10 ng ml<sup>-1</sup>), or TNF + IFN $\gamma$  with control (0.1% DMSO), Q-VD-OPh (20  $\mu$ M) with/without the RIPK1 inhibitor Nec-1s (10  $\mu$ M, **f**), RIPK3 inhibitor HS-1371 (2  $\mu$ M, **g**), and MLKL inhibitor GW806742X (2  $\mu$ M, **h**) (representative images shown; n = 3). **i**, normalized expression of selected genes in B16 cells treated with TNF (10 ng ml<sup>-1</sup>), IFN $\gamma$  (100 ng ml<sup>-1</sup>), or both, compared to control cells (source data for bulk RNA-seq – Manguso et al. 2017). **j**, normalized expression of *Mkl1* and *Ripk3* in control and *Tbkl*-null B16 cells with/without TNF/IFN $\gamma$  treatment (18 h) determined by qRT-PCR (n = 3; 2-way ANOVA, Sidak's multiple comparison test). \**P* < 0.05; \*\**P* < 0.01; \*\*\**P* < 0.001; \*\*\*\* *P* < 0.0001; *ns*, not significant. **k**, Western blot of indicated proteins in *Tbkl*-null B16 cell lysates following 2-hour pre-treatment with vehicle control (0.1%DMSO), Q-VD-OPh (20  $\mu$ M), Nec-1s (10  $\mu$ M), or Q-VD-OPh plus Nec-1s, or Q-VD-OPh plus birinapant (1  $\mu$ M) followed by 10 h treatment with TNF (160 ng ml<sup>-1</sup>) and IFN $\gamma$  (40 ng ml<sup>-1</sup>) or unstimulated (PBS) control. Data are representative of three independent experiments.



Extended Data Fig. 9 | See next page for caption.

**Extended Data Fig. 9 | Supporting data regarding TNF/IFN $\gamma$ -induced cell death signalling in control and *Tbk1*-null cells.** **a**, heatmap of % cytochrome C (cyt C) release for *in vitro* BH3 profiling of unstimulated control (sg1 and sg2) and *Tbk1*-null (sg1 and sg2) B16 cells. Mean values shown; n=3 biologically independent samples; 2-way ANOVA, Dunnett's multiple comparisons test. **b**, heatmap of % cytochrome C (cyt C) release for *in vitro* BH3 profiling of control sgRNA and *Tbk1* sgRNA B16 cells. Mean values shown; n = 3 biologically independent samples; 2-way ANOVA, Tukey's multiple comparisons test. No statistically significant differences observed between control sgRNA and *Tbk1* sgRNA B16 cells at any time point. **c**, Viability assessment (Cell Titer Glo) of B16 cells in standard 2D culture after 24 h treatment with indicated concentrations of staurosporine (STS) in control and *Tbk1*-null B16 cells. Means (bars) and individual values (open circles) are shown (n = 6, 2 independent experiments, 2-way ANOVA, Sidak's multiple comparisons test). **d**, Viability assessment (Hoechst/propidium iodide) of B16 tumour spheroids (lacking immune cells) in 3D microfluidic culture after 48 h treatment indicated concentrations of staurosporine (STS) compared to unstimulated cells. Means (bars) and individual values (open circles) are shown (n = 6, 2 independent experiments,

1-way ANOVA, Holm-Sidak's multiple comparisons test). **e**, Western blot for STING, IRF3, TBK1, and  $\beta$ -actin in B16 cells with single CRISPR cell lines with single-guide RNAs targeting *Tmem173*, *Irf3*, and *Tbk1* compared to control sgRNA. Data are representative of three independent experiments. **f**, Western blot for STING, IRF3, TBK1, and  $\beta$ -actin in double CRISPR B16 cells with indicated sgRNA pairs. Data are representative of three independent experiments. **g**, Viability assessment (Cell Titer Glo) of indicated sgRNA B16 cells after 48 h treatment with TNF (160 ng ml<sup>-1</sup>) + IFN $\gamma$  (40 ng ml<sup>-1</sup>) compared to unstimulated cells. Means (bars) and individual values (open circles) are shown (n = 4 biological replicates, 2-way ANOVA, Sidak's multiple comparisons test, \*\**P* < 0.01; \*\*\*\**P* < 0.0001; *ns*, not significant). **h**, PDOTS viability assessment from patients (n = 2) with cutaneous melanoma with indicated treatments. Means (bars) and individual values (open circles) are shown (n = 6 biological replicates, 2 independent specimens; one-way ANOVA with Dunn's multiple comparisons test, \*\**P* < 0.01; \*\*\*\**P* < 0.0001; *ns*, not significant). **i**, heatmap of secreted cytokine profiles (L2FC) of conditioned media from PDOTS in response to indicated treatments (n = 2). Mean values shown. \*\**P* < 0.01; \*\*\*\**P* < 0.0001; *ns*, not significant.



Extended Data Fig. 10 | See next page for caption.

**Extended Data Fig. 10 | Supporting data that IFN $\gamma$  sensing is essential for effector cytokine-induced death in TBK1-null cells.** **a**, Frequency histograms of enrichment (z-score) for all sgRNAs per target in a *Tbk1*-null B16 cells +/- *in vitro* stimulation with TNF (10 ng ml<sup>-1</sup>) and IFN $\gamma$  (10 ng ml<sup>-1</sup>). **b**, scatter plot depicting relative depletion of sgRNAs targeting 19,674 genes in a Cas9+ B16 control and *Tbk1* sgRNA cell line +/- *in vitro* stimulation with TNF (10 ng ml<sup>-1</sup>) and IFN $\gamma$  (10 ng ml<sup>-1</sup>). **c**, Western blot of control sgRNA and *Tbk1*-null B16 cells treated with TNF (160 ng ml<sup>-1</sup>) and IFN $\gamma$  (40 ng ml<sup>-1</sup>) for the indicates times. Data are representative of three independent experiments. **d**, cell viability assessment in parental B16 cells pre-treated with TBK1i (1  $\mu$ M) +/- JAK1/2 inhibitor (ruxolitinib, 0.5  $\mu$ M) +/- TNF/IFN $\gamma$  for 48 h compared to unstimulated controls. Means (bars) and individual values (open circles) are shown (n=3, 1

independent experiment; 2-way ANOVA, Dunnett's multiple comparisons test; \* $P < 0.05$ ; \*\*\* $P < 0.001$ ; \*\*\*\* $P < 0.0001$ ; *ns*, not significant). **e**, Western blot of indicated proteins in *Tbk1*-null B16 cell lysates following 2-hour pre-treatment with vehicle control (0.1%DMSO), ruxolitinib (1  $\mu$ M), Q-VD-OPh (20  $\mu$ M), Nec-1s (10  $\mu$ M), or Q-VD-OPh plus Nec-1s followed by 10-hour treatment with TNF (160 ng ml<sup>-1</sup>) and IFN $\gamma$  (40 ng ml<sup>-1</sup>) or unstimulated (PBS) control. Data are representative of three independent experiments. **f**, GR values for 9-point inhibitor titration of ruxolitinib (JAK1/2i) in parental, control sgRNA (monoclonal), and *Tbk1* sgRNA (monoclonal) B16 cells (2 independent experiments; representative data from single experiment with 6 technical replicates per condition). Means (solid circles) are shown +/- s.e.m (error bars).

## Reporting Summary

Nature Portfolio wishes to improve the reproducibility of the work that we publish. This form provides structure for consistency and transparency in reporting. For further information on Nature Portfolio policies, see our [Editorial Policies](#) and the [Editorial Policy Checklist](#).

### Statistics

For all statistical analyses, confirm that the following items are present in the figure legend, table legend, main text, or Methods section.

n/a Confirmed

- The exact sample size ( $n$ ) for each experimental group/condition, given as a discrete number and unit of measurement
- A statement on whether measurements were taken from distinct samples or whether the same sample was measured repeatedly
- The statistical test(s) used AND whether they are one- or two-sided  
*Only common tests should be described solely by name; describe more complex techniques in the Methods section.*
- A description of all covariates tested
- A description of any assumptions or corrections, such as tests of normality and adjustment for multiple comparisons
- A full description of the statistical parameters including central tendency (e.g. means) or other basic estimates (e.g. regression coefficient) AND variation (e.g. standard deviation) or associated estimates of uncertainty (e.g. confidence intervals)
- For null hypothesis testing, the test statistic (e.g.  $F$ ,  $t$ ,  $r$ ) with confidence intervals, effect sizes, degrees of freedom and  $P$  value noted  
*Give  $P$  values as exact values whenever suitable.*
- For Bayesian analysis, information on the choice of priors and Markov chain Monte Carlo settings
- For hierarchical and complex designs, identification of the appropriate level for tests and full reporting of outcomes
- Estimates of effect sizes (e.g. Cohen's  $d$ , Pearson's  $r$ ), indicating how they were calculated

*Our web collection on [statistics for biologists](#) contains articles on many of the points above.*

### Software and code

Policy information about [availability of computer code](#)

- Data collection
- Data analysis

For manuscripts utilizing custom algorithms or software that are central to the research but not yet described in published literature, software must be made available to editors and reviewers. We strongly encourage code deposition in a community repository (e.g. GitHub). See the Nature Portfolio [guidelines for submitting code & software](#) for further information.

### Data

Policy information about [availability of data](#)

All manuscripts must include a [data availability statement](#). This statement should provide the following information, where applicable:

- Accession codes, unique identifiers, or web links for publicly available datasets
- A description of any restrictions on data availability
- For clinical datasets or third party data, please ensure that the statement adheres to our [policy](#)

All data presented in this manuscript are available from the corresponding author upon reasonable request and will be deposited with appropriate accession codes before publication.

## Human research participants

Policy information about [studies involving human research participants and Sex and Gender in Research.](#)

Reporting on sex and gender	clinical specimens used for PDOTS were obtained from male and female patients and gender is indicated in Supplemental Table 1
Population characteristics	adult (age >18) patients with advanced malignancies (solid tumours) treated at MGH or DFCl
Recruitment	The research conducted involved secondary research using de-identified data and biospecimens collected as part of routine clinical care and not collected specifically for this study.
Ethics oversight	Because the specimens or data were not collected specifically for this study and no one on the study team had access to the subject identifiers linked to the specimens or data, this study is not considered human subjects research. IRB-approved protocols were used for the procurement of de-identified patient samples by the MGH Melanoma Tissue Repository (PI: Dr. Genevieve M. Boland). Informed consent was obtained from all subjects and blood/tissue samples were collected and analyzed according to Dana-Farber/Harvard Cancer Center IRB-approved protocols (DF/HCC 11-181, 02-240, and 13-416). These studies were conducted according to the Declaration of Helsinki and approved by the DFHCC IRB. All samples will be labeled with a unique 5-digit code without any patient identifiers.

Note that full information on the approval of the study protocol must also be provided in the manuscript.

## Field-specific reporting

Please select the one below that is the best fit for your research. If you are not sure, read the appropriate sections before making your selection.

Life sciences  Behavioural & social sciences  Ecological, evolutionary & environmental sciences

For a reference copy of the document with all sections, see [nature.com/documents/nr-reporting-summary-flat.pdf](https://www.nature.com/documents/nr-reporting-summary-flat.pdf)

## Life sciences study design

All studies must disclose on these points even when the disclosure is negative.

Sample size	Group sizes for in vivo validation experiments were selected empirically based upon prior knowledge of the intragroup variation of tumor challenges and immunotherapy treatment. Sample sizes for in vivo mouse experiments were chosen based on previous experience in similar studies (Manguso et al. Nature 2017). Similarly, group sizes in vitro were selected on the basis of prior knowledge of variation (e.g. for growth/viability assays). For PDOTS studies, assuming an overall comparison-wide type-I error of 0.1 (2-sided) and sample of size 35, each pairwise comparison would have at least 85% power to detect a difference in expression that is approximately 0.8 times the common standard deviation (effect size=0.8). Based on prior data, we expected a null rate of 25%. A treatment would be considered promising if at least 50% of patient samples achieved response. Statistical assessments were based on one-sample, exact binomial tests, with an overall, two-sided alpha=0.1 divided equally among the three treatment comparisons. With 35 patient samples, there would be approximately 85% power to detect the difference between response rates of 25% and 50%. A p value less than 0.05 will be the cut off for statistical significance. Statistical analysis was performed after n=30 PDOTS and found to be statistically significant.
Data exclusions	No data were excluded from the experiments
Replication	Replicates were used in all experiments as noted in text, figure legends and methods. All in vivo experiments were repeated at least twice with consonant results, with the exception of those that were supporting/confirmatory in nature and appear ONLY in Extended Data (e.g. Size Match experiment). All experiments presented for which replication was attempted were successfully replicated.
Randomization	Mice were age and sex-matched and randomized where appropriate (e.g. prior to initiating treatment for matched conditions). For PDOTS studies, samples were acquired based on specimen availability over the course of the study. The number of treatment groups for each PDOTS experiment was determined based on sample size/quality as assessed by the operator, with larger specimens facilitating larger numbers of treatment groups. Each specimen was treated with at least anti-PD-1, TBK1i, anti-PD-1 plus TBK1i, compared to untreated control, with additional treatments (e.g., TNFa/IFNg) as tissue specimen availability permitted. For GR metrics studies,
Blinding	Investigators were not blinded to treatment groups or genotypes for in vivo or in vitro studies, as knowledge of this information was essential to conduct the studies. For animal studies, no blinding was performed due to requirements for cage labeling and staffing needs.

## Reporting for specific materials, systems and methods

We require information from authors about some types of materials, experimental systems and methods used in many studies. Here, indicate whether each material, system or method listed is relevant to your study. If you are not sure if a list item applies to your research, read the appropriate section before selecting a response.

## Materials &amp; experimental systems

n/a	Involved in the study
<input type="checkbox"/>	<input checked="" type="checkbox"/> Antibodies
<input type="checkbox"/>	<input checked="" type="checkbox"/> Eukaryotic cell lines
<input checked="" type="checkbox"/>	<input type="checkbox"/> Palaeontology and archaeology
<input type="checkbox"/>	<input checked="" type="checkbox"/> Animals and other organisms
<input checked="" type="checkbox"/>	<input type="checkbox"/> Clinical data
<input checked="" type="checkbox"/>	<input type="checkbox"/> Dual use research of concern

## Methods

n/a	Involved in the study
<input checked="" type="checkbox"/>	<input type="checkbox"/> ChIP-seq
<input type="checkbox"/>	<input checked="" type="checkbox"/> Flow cytometry
<input checked="" type="checkbox"/>	<input type="checkbox"/> MRI-based neuroimaging

## Antibodies

## Antibodies used

## Flow cytometry -

anti-mouse CD45 BV605 (clone 30-F11, BioLegend, #103139), 1:50 dilution  
 anti-mouse F4/80 (clone QA17A29, BioLegend, #157306), 1:100 dilution  
 anti-mouse CD8a BV785 (clone 53-6.7, BioLegend, #100749), 1:100 dilution  
 anti-mouse CD4 PerCP (clone RM4-5, BioLegend, #100538), 1:50 dilution  
 anti-mouse NK-1.1 BV421 (clone PK136, Invitrogen, #404-5941-82), 1:50 dilution  
 anti-mouse TCR $\beta$  APC-Cy7 (clone H57-597, BioLegend, #109220), 1:50 dilution  
 anti-mouse FoxP3 (clone FJK-16s, Invitrogen, #12-5773-82), 1:50 dilution  
 anti-human/mouse Granzyme B FITC (clone GB11, BioLegend, #515403), 1:100 dilution  
 anti-mouse CD69 BV421 (#104527, clone H1.2F3, BioLegend), 1:20 dilution  
 anti-CD25 AF700 (#102024, clone PC61, BioLegend), 1:20 dilution  
 anti-IFN $\gamma$  PE (#505807, clone XMG1.2, BioLegend), 1:20 dilution  
 anti-TNF $\alpha$  FITC (#506303, clone MP6-XT22, BioLegend), 1:20 dilution  
 anti-IL-2 PerCP/Cy5.5 (#503821, JES6-5H4, BioLegend), 1:20 dilution

## Western blotting:

TBK1 (#ab40676, Abcam)  
 IKKepsilon (#3416T, Cell Signaling)  
 p-RIPK S166/T169 (#31122S, Cell Signaling)  
 RIPK1 (#3493S, Cell Signaling)  
 cleaved caspase 8 (#9429S, Cell Signaling)  
 cleaved caspase 3 (#9661T Cell Signaling)  
 cleaved PARP (#6544, Cell Signaling)  
 c-FLIP (#56343S, Cell Signaling)  
 p-STAT1 Y701 (#9167S, Cell Signaling)  
 STAT1 (#14994S, Cell Signaling)  
 STING (#13647S, Cell Signaling)  
 p-IRF3 (#29047S, Cell Signaling)  
 IRF3 (#4302S, Cell Signaling)  
 p-JAK1 (#74129T, Cell Signaling)  
 JAK1 (#3344T, Cell Signaling)  
 p-JAK2 (#8082T, Cell Signaling)  
 JAK2 (#3230T, Cell Signaling)  
 p-p65 (#3033T, Cell Signaling)  
 p65 (#8242T, Cell Signaling)  
 p-MLKL S345 (#37333, Cell Signaling)  
 MLKL (#37705, Cell Signaling).  
 beta-actin-680 (#MA5-15739-D680, Invitrogen)  
 Primary antibodies were used at 1:1000 dilution in LI-COR Blocking Buffer.  
 IRDye secondary antibodies against rabbit IgG, mouse IgG or goat IgG were purchased from LI-COR Biosciences (Invitrogen) and used at 1:10,000.

## In vivo/ex vivo studies

isotype control IgG2a,k (#BE0089, clone 2A3, BioXCell), 10mg/kg in vivo, 10 ug/mL ex vivo (MDOTS)  
 rat monoclonal anti-PD1 antibodies (#BP0273, BioXCell, clone: 29F.1A12), 10mg/kg in vivo, 10 ug/mL ex vivo (MDOTS)  
 anti-human PD-1 IgG4 (pembrolizumab, Merck) - 250 ug/mL final concentration (PDOTS), 1:100 dilution of 25 mg/mL stock  
 anti-human CTLA-4 IgG1 (ipilimumab, BMS) - 50 ug/mL final concentration (PDOTS), 1:100 dilution of 5 mg/mL stock  
 Control human IgG4 (Invivogen, anti- $\beta$ -gal-hlgG4 (bgal-mab114) 100 ug/mL final (PDOTS)

## Validation

For Western Blots, antibody validation is included in the Main Figures and Extended Data Figures, which demonstrate positive control and knockout samples on the same blot. Antibody validation for TBK1 was performed using CRISPR/knockout cell lines (Fig. 5a, 5f, e1b) and over expression of V5-tagged wild-type TBK1 (data not shown). Validation for flow antibodies was shown previously (Ishizuka et al. Nature 2018). Further validation is present on the manufacturer's website as noted in the Methods section.

## Eukaryotic cell lines

Policy information about [cell lines and Sex and Gender in Research](#)

## Cell line source(s)

B16.F10, CT26, and A375 cell lines were purchased from ATCC. B16-ova were obtained from D. Sen. GVAX was a gift from G.

Cell line source(s)	Dranoff. Braf/Pten (D4M.3A) melanoma cell line was obtained from D.E. Fisher. A375-CR cells were provided by G. Zhang. MB49 cells (used for in vivo studies only) were licensed from Dr. K Esuvaranathan (University of Singapore) by vivoPharm in collaboration with Gilead Sciences.
Authentication	A375 and A375-CR (resistant) human melanoma cells lines were authenticated using STR profiling. STR profiling was not performed on murine cancer cell lines (B16, D4M.3A, CT26, MC38, MB49).
Mycoplasma contamination	All cell lines were routinely tested for mycoplasma. None of the cell lines used in this study have tested positive for mycoplasma.
Commonly misidentified lines (See <a href="#">ICLAC</a> register)	None

## Animals and other research organisms

Policy information about [studies involving animals](#); [ARRIVE guidelines](#) recommended for reporting animal research, and [Sex and Gender in Research](#)

Laboratory animals	Wild-type female C57BL/6J mice (7 weeks old) were obtained from Jackson Laboratories. A colony of NOD.Cg-Prkdcscid Il2rgtm1Wjl/SzJ (NSG) mice were bred on site at the Broad Institute. Mice were age-matched to be 6–12 weeks old at the time of tumour inoculation. Wild-type female C57BL/6J mice (7-8 weeks old) were obtained from Charles River Laboratories for TBK1i in vivo studies. B16 and B16-ova MDOTS were prepared from tumours using wild-type female C57BL/6J mice (6 weeks old, Jackson Labs). D4M.3A (Braf/Pten) MDOTS were generated using wild-type male C57BL/6J mice (6 weeks old, Jackson Labs). CT26 MDOTS were prepared using wild-type female BALB/c mice (6-8 weeks old, Jackson Labs). Housing - Innovive® individually ventilated cages. Acclimation - 2 days. Food - ad libitum, Teklad® Global 18% Protein Rodent Diet, irradiated. Water - Sterile prefilled bottles. Dark/Light cycle on a 12 hour automated schedule. Temperature ambient and humidity within parameters of IACUC guidelines 30-70%.
Wild animals	No Wild animals were used in this study
Reporting on sex	Mice were age and sex-matched. Male and female mice were used for specific syngeneic models as indicated.
Field-collected samples	No Field-collected samples were used in this study
Ethics oversight	IACUC committee of the Broad Institute of Harvard and MIT and Charles River Laboratories

Note that full information on the approval of the study protocol must also be provided in the manuscript.

## Flow Cytometry

### Plots

Confirm that:

- The axis labels state the marker and fluorochrome used (e.g. CD4-FITC).
- The axis scales are clearly visible. Include numbers along axes only for bottom left plot of group (a 'group' is an analysis of identical markers).
- All plots are contour plots with outliers or pseudocolor plots.
- A numerical value for number of cells or percentage (with statistics) is provided.

### Methodology

Sample preparation	Tumor-infiltrating lymphocytes were stained directly from single-cell preparations of explanted murine tumors as described in the materials and methods.
Instrument	CytoFLEX LX Flow Cytometer (Beckman Coulter).
Software	FlowJo (v10)
Cell population abundance	Tumour-infiltrating lymphocytes were enriched by CD45+ MACS positive selection (Miltenyi Biotec).
Gating strategy	All gates were set based on FMO (full-minus one) stains and isotype control antibodies after appropriate compensation using single-stained compensation controls. This will be provided as supplemental information in a revised version before publication.

- Tick this box to confirm that a figure exemplifying the gating strategy is provided in the Supplementary Information.